# Development of Integrated Modeling Tools for Used Fuel Repository Natural Barrier Evaluations

## Fuel Cycle Research & Development

*Prepared for*
*U.S. Department of Energy*
*Used Fuel Disposition Campaign*

***Scott L Painter, Dylan R Harp, Shaoping Chu, Satish Karra, Nataliia Makedonska and Terry Miller***
*Los Alamos National Laboratory*
***Teklu Hadgu, Payton Gardner and Yifeng Wang***
*Sandia National Laboratory*

*September 2013*

**FCRD-UFD-2013-000375**
**LA-UR-13-27517**

Revision 1
08/19/2011

FCT Quality Assurance Program Document

# Appendix E
# FCT Document Cover Sheet

| | |
|---|---|
| Name/Title of Deliverable/Milestone | Development of Integrated Modeling Tools for Used Fuel Repository Natural Barrier Evaluations |
| Work Package Title and Number | M3FT-13LA0807046 Report on Integrated Tool Development for Natural System Evaluations |
| Work Package WBS Number | ActivityFT-13LA0807045 |
| Responsible Work Package Manager | Scott Painter (Name/Signature) |
| Date Submitted | 9/30/2013 |
| Quality Rigor Level for Deliverable/Milestone | ☒ QRL-3 ☐ QRL-2 ☐ QRL-1 ☐ N/A* ☐ Nuclear Data |
| This deliverable was prepared in accordance with | Los Alamos National Laboratory *(Participant/National Laboratory Name)* |
| QA program which meets the requirements of | ☒ DOE Order 414.1 ☐ NQA-1-2000 ☐ Other |

**This Deliverable was subjected to:**

| | |
|---|---|
| ☒ Technical Review | ☐ Peer Review |
| **Technical Review (TR)** | **Peer Review (PR)** |
| **Review Documentation Provided** | **Review Documentation Provided** |
| ☐ Signed TR Report or, | ☐ Signed PR Report or, |
| ☐ Signed TR Concurrence Sheet or, | ☐ Signed PR Concurrence Sheet or, |
| ☒ Signature of TR Reviewer(s) below | ☐ Signature of PR Reviewer(s) below |
| **Name and Signature of Reviewers** | |
| Ethan Coon | |

***NOTE** *In some cases there may be a milestone where an item is being fabricated, maintenance is being performed on a facility, or a document is being issued through a formal document control process where it specifically calls out a formal review of the document. In these cases, documentation (e.g., inspection report, maintenance request, work planning package documentation or the documented review of the issued document through the document control process) of the completion of the activity along with the Document Cover Sheet is sufficient to demonstrate achieving the milestone. QRL for such milestones may also be marked N/A*

# EXECUTIVE SUMMARY

The natural barrier system is an integral part of a geologic nuclear waste repository. Spatially, it extends from a disturbed rock zone created by mechanical, thermal and chemical perturbations due to underground excavation or waste emplacement through the surrounding geologic media to the specified repository boundary. From the well accepted multiple barrier concept for waste repository safety, each barrier is to be independently utilized for its safety function. For this reason, the natural barrier needs to be evaluated to ensure adequate safety function. The work described in this report is intended to ensure that the computational tools are available to more realistically evaluate NBS performance and take appropriate performance credit for natural barriers.

This report describes work to develop integrated modeling frameworks that can be used to systematically analyze the performance of a natural barrier system and identify key factors that control the performance of the system. The frameworks are designed as an integrated tool for prioritization and programmatic decisions of UFDC natural system R&D activities. In addition, the computational strategies developed will be useful for the development of total system modeling capabilities within the generic disposal system analysis work package.

The integrated tool development for natural system evaluation adopts a phased approach. This report documents the results of FY2013 activities, which were focused on demonstrating integrated analyses of natural barriers in generic salt and granite repositories. Robust strategies for integrated modeling were refined and deployed. Modern parallel modeling tools for subsurface flow and transport were coupled with constrained and unconstrained uncertainty analysis tools in both examples. The two examples demonstrate that higher fidelity representations of natural-system processes are feasible within a disposal system analyses framework.

# CONTENTS

# FIGURES

# TABLES

# DEVELOPMENT OF INTEGRATED MODELING TOOLS FOR USED FUEL REPOSITORY NATURAL BARRIER EVALUATIONS

## 1. INTRODUCTION

The natural barrier system is an integral part of a geologic nuclear waste repository. Spatially, it extends from a disturbed rock zone created by mechanical, thermal and chemical perturbations due to underground excavation or waste emplacement through the surrounding geologic media to the specified repository boundary.

From the well-accepted multiple barrier concept for waste repository safety, each barrier is to be independently utilized for its safety function. For this reason, the natural barrier needs to be evaluated to ensure adequate safety function. From a repository design point of view, an appropriate balance in terms of contribution to the total system performance must be maintained between the natural barrier system (NBS) and the engineered barrier system (EBS). In practice, there is a risk that too much reliance is placed on the engineered barrier while not fully taking credit for the barrier function of the natural system. Such practice often results in overly conservative and unnecessarily expensive EBS designs. The work described in this report is intended to ensure that the computational tools are available to more realistically evaluate NBS performance and take more performance credit for natural barriers.

### 1.1 Objectives

The overall objective of the work described in this report is to evaluate and demonstrate computational tools that will be required to take more realistic credit for natural barrier performance within broader system-level analyses. In that sense, the work demonstrates more realistic subsystem evaluations and also provides guidance and accumulated experience on subsystem performance assessment for use in designing more realistic total system evaluation frameworks. The Phase I report on this activity (Wang et al. 2012) provided information on software choices and coupling strategies. This report applies those development efforts in applications to generic salt and granite repositories.

A detailed research plan was developed for the NBS evaluation and tool development and updated in FY2012 (Wang, 2012). The current work addresses 3 of the 27 priority topics identified in the research plan: Topic S2, disposal concept development; Topic S3, disposal system modeling; and Topic S4, development of a centralized technical database.

More broadly, this work supports two of the main objectives of the Used Fuel Disposition Campaign (UFDC) (Nutt, 2012):

1. Develop a fundamental understanding of disposal system performance in a range of environments for potential wastes that could arise from future nuclear fuel cycle alternatives through theory, simulation, testing, and experimentation.
2. Develop a computational modeling capability for the performance of storage and disposal options for a range of fuel cycle alternatives, evolving from generic models to more robust models of performance assessment.

### 1.2 Technical Approach

The integrated tool development for NBS evaluation follows a probabilistic approach, analogous to the one developed for a total system performance assessment (TSPA) (Helton et al., 1999). The United States Nuclear Regulatory Commission website (http://www.nrc.gov/about-nrc/regulatory/performance-assessment.html) provides a succinct definition of *performance assessment* for a disposal facility as:

*a quantitative evaluation of potential releases of radioactivity from a disposal facility into the environment, and assessment of the resultant radiological doses.*

Although several variants of this basic definition have been offered (e.g. Campbell and Cranwell, 1988; Nuclear Energy Agency, 1990; Gallegos and Bonano, 1993; and Ewing *et al*. 1999), in practice performance assessments generally have three major attributes:

1. the focus is on radionuclide releases and comparisons with appropriate standards
2. the scope of the analyses may vary from total system to subsystem (i.e. geologic barriers)
3. methods of uncertainty analysis are used to assess uncertainty in outcomes

The focus of this development effort is on the natural barrier subsystem with a view toward using more detailed process models (with appropriate levels of fidelity) for flow field and radionuclide transport calculations in a probabilistic performance assessment framework. In this framework, one or more detailed process models may be linked and wrapped by a probabilistic performance assessment driver (PPAD). The PPAD then drives probabilistic performance assessment calculations by sampling uncertain model input parameters and invoking Monte-Carlo simulations using the linked process model(s). It is important for the modeling framework to be flexible enough to accommodate various alternative models. This can be done through a *plug-and-play* technique.

Harp and Painter (2012) proposed some design principles for next-generation system and subsystem performance assessment frameworks (see also Section 2 of Wang et al. 2012):

1. Provide a flexible and extensible framework where alternative, existing process models and uncertainty analysis approaches can be interchanged in a plug-and-play structure;
2. Use a common data format for efficient data storage, processing, and organization;
3. Incorporate parallel and concurrent simulations (HPC) wherever possible;
4. Use calibration-constrained uncertainty analyses wherever possible;
5. Use sampling-based uncertainty analysis wherever calibration-constrained uncertainty analysis is not possible;
6. Use radionuclide transport algorithms that are tailored for performance assessments.

Principles 1 and 2 facilitate the use and exploration of various simulators and analyses within a given NBS subsystem assessment. A common data format discussed in principle 2 ensures that principle 1 is possible. Of course, the realization of principle 1 will require more than a common data format alone. The inclusion of complex physics-based models and uncertainty analyses should not be precluded from an assessment solely on the basis of computational constraints. In situations where complex models and analyses are appropriate and justified, an assessment should make use of these models. Principle 3 attempts to ensure that computational constraints do not limit the complexity of models and analyses by suggesting that parallel simulators and concurrent model evaluation be used whenever necessary. Assessments should utilize available data to constrain uncertainty (principle 4). In an actual application, it is likely that sparse hydraulic head measurements will be available from site characterization activities. These head measurements are typically not sufficient to fully specify the groundwater velocity but they do provide important constraints on the present-day flow field. Sparse measurements on groundwater age or other groundwater chemistry information provide similar partial constraints. Methods for producing multiple realizations of the permeability field that are consistent with partial constraints – calibration-constrained uncertainty analysis – are needed for this step. Principle 5 suggests that in cases where data are not available for calibration-constrained uncertainty analysis, sampling based uncertainty analyses should be used. The current availability of radionuclide transport algorithms specifically designed to work in an assessment framework should be used whenever possible (principle 6).

The work described in this report generally follows the six design principles listed above. A generic salt repository example and a generic granite repository example are used to refine and demonstrate the approach.

## 1.3 Structure of This Report

This report is structured as follows:

Section 1 described the concept and objectives of the report (Contributors: Scott Painter, LANL, and Yifeng Wang, SNL).

Section 2.0 describes the development of an integrated process modeling framework for natural system evaluation using an optimization code (PEST) and unconstrained uncertainty sampling code (PyMADS) a parallelized reactive transport code (PFLOTRAN) and sequential codes (Walkabout, MARFA). The framework is then applied to a granite repository environment. This section also discusses calibration-constrained uncertainty analyses using null-space Monte Carlo simulations. (Contributors: Dylan R. Harp, Satish Karra, Terry Miller, Nataliia Makedonska, Shaoping Chu, and Scott Painter, LANL)

Section 3.0 describes the development of an integrated process-modeling framework using DAKOTA and PFLOTRAN with application of this framework to a generic salt repository. (Contributors: Teglu Hadgu, Payton Gardner, and Yifeng Wang, SNL)

Section 4.0 provides the summary of the FY13 work and the future direction. (Contributors: Scott Painter, LANL, and Yifeng Wang, SNL)

## 1.4 References

Campbell, J.E. and Cranwell, R.M., 1988. Performance assessment of radioactive waste repositories. *Science*, **239**(18 March), pp. 1389–1392.

Ewing, R.C., Tierney, M.S., Konikow, L.F., Rechard, R.P., 1999. Performance assessments of nuclear waste repositories: A dialogue on their value and limitations. *Risk Analysis* **19**(5), pp. 933–958.

Harp, D.R., Painter, S.L., 2012. Report on Integrated Tool Development for Natural System Evaluation: LANL Input. Los Alamos National Laboratory, LA-UR-12-24251.

Helton, J.C., 1993. Uncertainty and sensitivity analysis techniques for use in performance assessment for radioactive waste disposal. *Reliability Engineering and System Safety*, **42**(2-3), pp. 327–367.

Gallegos, D.P., Bonano, E.J., 1993. Consideration of uncertainty in the performance assessment of radioactive waste disposal from an international regulatory perspective. *Reliability Engineering and System Safety*, **42**(2-3), pp. 111–123.

Nuclear Energy Agency, 1990. Disposal of High-Level Radioactive Wastes: Radiation Protection and Safety Criteria. In: NEA Workshop, Paris, 5-7 November 1990. NEA, Organisation for Economic Co-Operation and Development, Paris, 1991, Paris.

Nutt, M., 2012. Used Fuel Disposition Campaign Disposal Research and Development Roadmap, FCRD-USED-2011-000065, Rev 1.

Wang, Y., Hadgu, T., Painter, S., Harp, D. R., Chu, S., Wolery, T. and Houseworth, J., 2012. Integrated Tool Development for Used Fuel Disposition Natural System Evaluation – Phase I Report by September 28, 2012, FCRD-UFD-2012-000229, SAND2012-7073P. Milestone: M2FT-12SN0807081, Work Package: FT-12SN080708.

Wang, Y., 2012. Research & Development (R&D) Plan for Used Fuel Disposition Campaign (UFDC) Natural System Evaluation and Tool Development (Revision 1). FCRD-UFD-2013-000144.

# 2. INTEGRATED MODELING OF RADIONUCLIDE TRANSPORT IN THE FAR-FIELD OF A GENERIC GRANITE REPOSITORY

## 2.1 Generic Granite Repository Concept and Integrated Tool Design

### 2.1.1 Model Structure

A hypothetical repository situated in fractured granite is considered. Details of the EBS system are not relevant here, although the KBS-3 concept with bentonite buffers surrounding waste packages may be used to fix the concept. As is typical for fractured-rock sites, it is assumed that site characterization data only partially constrains the groundwater flow field. Moreover, the highly channelized nature of flow in fractured rock is assumed to lead to discrete transport pathways that link locations of failed waste packages to the biosphere.

Six sequentially linked process groups can be identified (Figure 2-1) as necessary for quantifying performance and assessing uncertainty in a generic granite repository. In an assessment framework, process-resolving software is associated with each group of processes. The terminology "process resolving software" (PRS) is used there to refer to stand-alone and possibly pre-existing process modeling software that represents a small number of relatively tightly coupled processes. Each PRS is part of a model chain, and is loosely coupled with upstream and downstream PRSs in the model chain. In the proposed framework, PRS1 simulates groundwater flow. PRS2 simulates evolution of the groundwater chemistry upstream of the engineered barrier system. If the groundwater flow system is adequately represented as steady over the time frame of interest and thermal perturbations of the flow and chemical system are modest, then this step is not necessary because measured groundwater chemistry may be used instead of simulated chemistry. However, if transient flow or thermal perturbations are to be modeled then simulation of chemistry in future climates may be needed. PRS3 simulates thermal conditions. PRS4 involves degradation of engineered barriers, release of radionuclides from the waste form, and transport of radionuclides through the EBS. This step is beyond the scope of this report, but is mentioned here because it couples to the geosphere through the effect of groundwater chemistry on EBS degradation, the thermal conditions in the EBS and in the near field, and the release of radionuclides. PRS5 represents carrier-plume reactive transport, the evolution of groundwater chemistry downstream of a failed waste package including the effects of EBS degradation products and thermal perturbations. PRS6 is radionuclide transport, possibly taking into account the effect of major ion chemistry calculated from PRS5. The separation of radionuclide transport (PRS6) from major ion chemistry (PRS5) is consistent with the expected low concentrations of radionuclides in the geosphere such that radionuclides do not significantly influence the overall solution chemistry. It is important to note, however, that one-way coupling is represented. Thus, the concentration of complexing agents as calculated by PRS5 may influence equilibrium distribution coefficients. If surface complexation models are used to calculate radionuclide immobilization, the parameters appearing in those models may be calculated from the output of PRS5. This separation into two process kernels is computationally expedient given that the application requires dozens of radionuclides to be represented. One-way coupling is generally a good approximation in the repository far field because radionuclide concentrations are typically too small to significantly influence the bulk chemistry.

The structure of the framework shown in Figure 2-1 has two prominent features. The first structural feature is that the six PRSs are arranged into two loops. In the first loop, ambient groundwater flow and chemistry PRSs are called in a calibration constrained uncertainty loop. This analysis will produce alternative flow fields that are all consistent with the available constraints on hydraulic head, groundwater age, etc. In the second loop, unconstrained (sampling based) uncertainty analysis is used to drive the remaining model chain in a more traditional assessment mode. The second structural feature is that the PRSs are not passing data directly among themselves. Instead, each is reading from and writing to a common data layer. This feature is essential to the plug and play nature of the framework, as it allows

process kernels to be replaced without initiating a cascading set of changes in the PRSs upstream and downstream in the workflow.

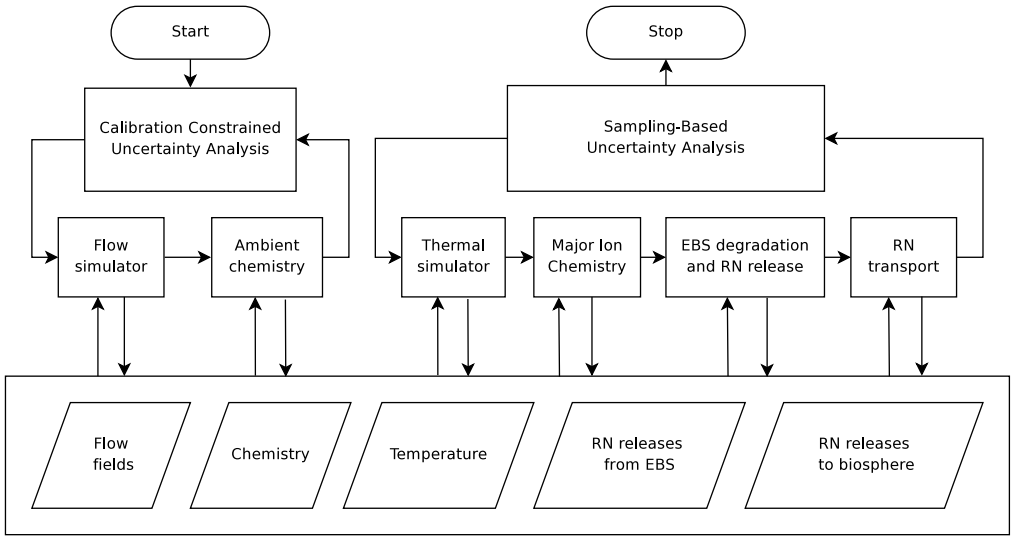


**Figure 2-1. Schematic of an Integrated Modeling Framework for Natural Barrier Evaluation.**

### 2.1.2 Process Resolving Software

Groundwater flow (PRS1) was modeled using PFLOTRAN (Lichtner et al., 2013). PFLOTRAN is a high-performance parallel flow and reactive transport simulator. PFLOTRAN was used in the integrated assessment to produce velocity fields for heterogeneous permeability fields. A workflow was developed for this project to produce PFLOTRAN unstructured mesh files from LaGriT (LaGriT, 2013) mesh files. Modifications were made to PFLOTRAN to produce the appropriate output for flow path construction. The use of PFLOTRAN in an integrated assessment makes it possible to utilize parallel computing resources. Although not used here, PFLOTRAN also has the ability to simulate flow in discrete fracture networks.

Although PFLOTRAN has the capability to model radionuclide transport (PRS6) in a conventional finite-difference framework (see Section 3 of this report), that classical numerical approach is computationally demanding for advection-dominated systems. Solute diffusion into matrix blocks compounds the computational requirements. An alternative approach was used here wherein purely advective particle tracking was first used to define transport pathways, and then radionuclide transport was simulated along the pathway using a highly robust semi-analytical Monte Carlo method.

Walkabout (Painter, 2011) was used to construct flow paths from velocity fields. Walkabout performs random walk particle tracking simulations of solute transport based on groundwater flow solutions that use fully unstructured control volume grids. The first step in Walkabout is the reconstruction of the velocity field to cell centers, which enables interpolation of the velocity to any point in the model domain. Walkabout then uses a first-order predictor-corrector method weighted to the corrector to compute the advective displacement. If an advective displacement moves the particle across a no-flow boundary, the

time step is recursively decreased until the displacement does not cross the boundary. Modifications were made to Walkabout for this project to read and write in formats consistent with the data layer.

Radionuclide transport was simulated using the MARFA code (Painter and Mancillas, 2013). MARFA simulates radionuclide transport in a sparsely fractured geologic medium using a Monte Carlo approach wherein non-interacting particles represent packets of radionuclide mass. MARFA includes the ability to model advection, longitudinal dispersion, Fickian diffusion into an infinite or finite rock matrix, equilibrium sorption, decay, and in-growth. MARFA produces particle arrival times at the surface, which can be used to calculate cumulative mass discharge at the surface at a given time. Groundwater velocity, aperture, and retention parameters along the predefined pathways compose the input to MARFA.

### 2.1.3 Uncertainty Analyses

PEST (Doherty *et al.* 1994) was used to perform Null-Space Monte Carlo (NSMC, e.g. Tonkin and Doherty, 2009) to obtain a set of velocity fields constrained to available head observations while considering uncertainty in the permeability field. NSMC provides an approximation of model uncertainty in a computationally efficient manner using subspace techniques to reduce the dimensionality of the parameter space. The use of Parallel PEST (PPEST) allowed parallel computing resources to be used for concurrent model simulation.

Latin Hypercube Sampling (LHS) was performed using the Bayesian-Inference Python package (Coelho et al 2013) and the LANL-developed PyMADS, a python package for the Model Analysis and Decision Support (MADS) software (Vesselinov *et al.* 2013). The Bayesian-Inference package implements several probabilistic parameter distributions and allows parameter correlations to be included in the sampling. LHS was used to sample retention properties in the radionuclide transport simulations. PyMADS uses Parallel Python (Vanovshi, 2010) to schedule and execute simulations on a variety of computing resources (multiprocessor workstations, servers, and clusters).

## 2.2 Demonstration Example

### 2.2.1 Scenario and Workflow

A hypothetical site with characteristics similar to typical granite repository sites was considered. The site has a constant infiltration of 100 mm/y along the top and side of a hill and discharge to a topographically depressed region representing a shallow lake. The infiltration forces flow through a hypothetical repository location. Flow to the depression is enhanced by the presence of an intensely fractures deformation zone with enhanced porosity and permeability. This conceptual model was realized in a 2D model domain 1000 m × 1 m in x and y (horizontal) dimensions and from 550 to 600 m in the z (vertical) dimension. Figure 2-2 shows the material zones and boundary faces of the numerical model. The outflow face pressure was held fixed at atmospheric pressure. The permeability of the deformation zone was fixed at $10^{-10}$ $m^2$, while the permeabilities of the background rock and repository zones were modeled as random space functions. A spherical variogram with a range of 400 m in the horizontal (x) direction and 100 m in the vertical (z) direction was assumed.

When deploying the integrated framework to assess a site, it is expected that hydraulic head measurements will be available, thereby partially but not completely constraining the flow fields. Thus, calibration constrained uncertainty assessment is needed, as described in Section 1.2. To explore how this would work in practice, a synthetic truth permeability field was constructed. To that end, 27 conditioning points were distributed between z = 150 m and z = 450 m and assigned uniform random values between $10^{-14}$ and $10^{-10}$ $m^2$. Figure 2-3 shows the locations of the conditioning points and the 'true' permeability field. Porosity is fixed at 0.01 in the deformation zone and 0.001 in the background rock and repository zones. It was then assumed that hydraulic heads are available at the 115 locations in 6 wells shown in Figure 2-4. The observations were distributed at approximately 10 m intervals along the wells. The

observations do not form perfectly straight vertical lines as the observation locations were selected at cell centers of the unstructured mesh nearest to the well.

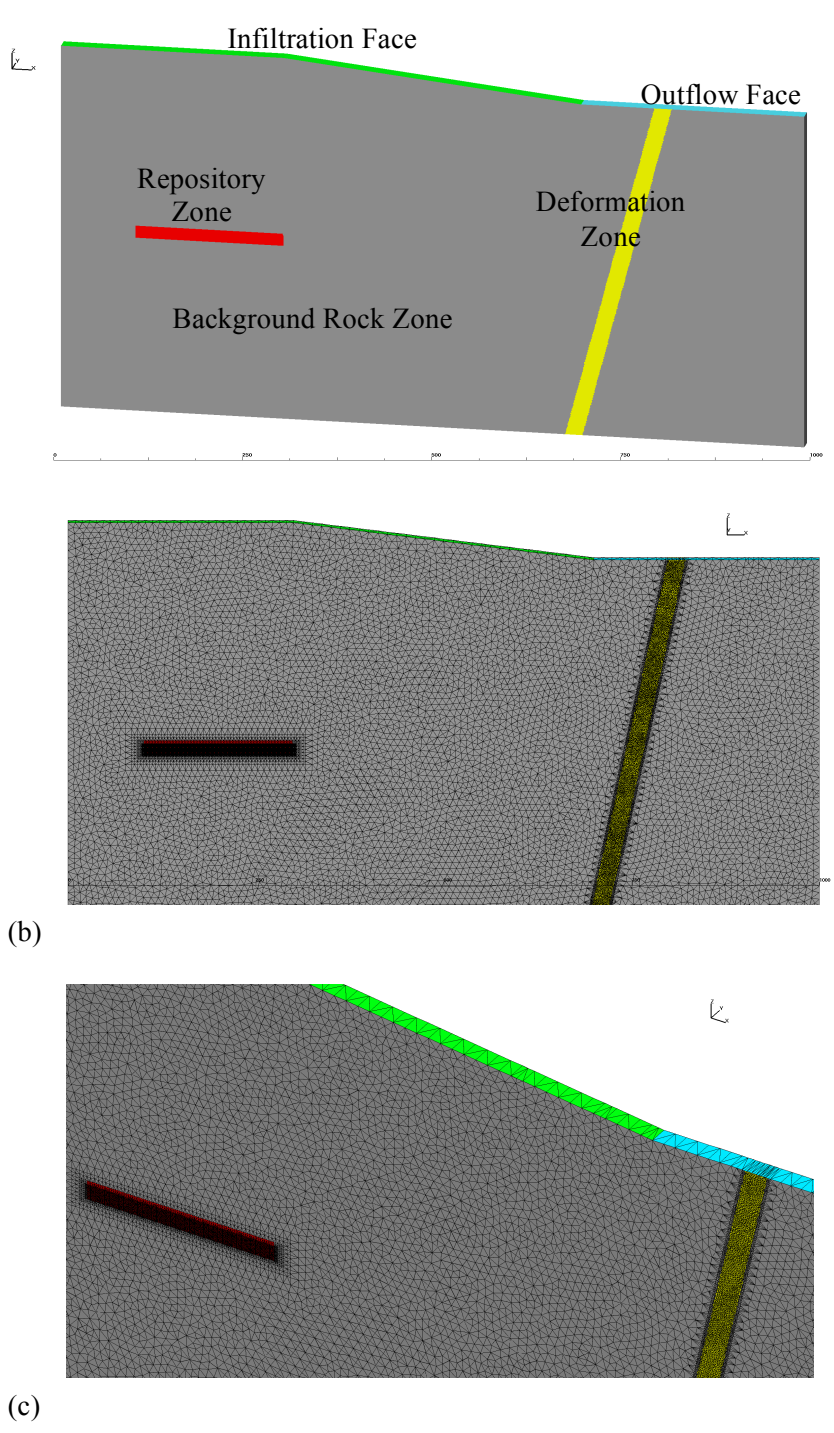


**Figure 2-2. (a) Material zones and faces of scenario (shown in 3D perspective). (b) 2D slice of model with mesh (Delaunay triangulation indicating connectivity) (c) Close up of top of model where infiltration and outflow faces meet. Length scales are in meters.**

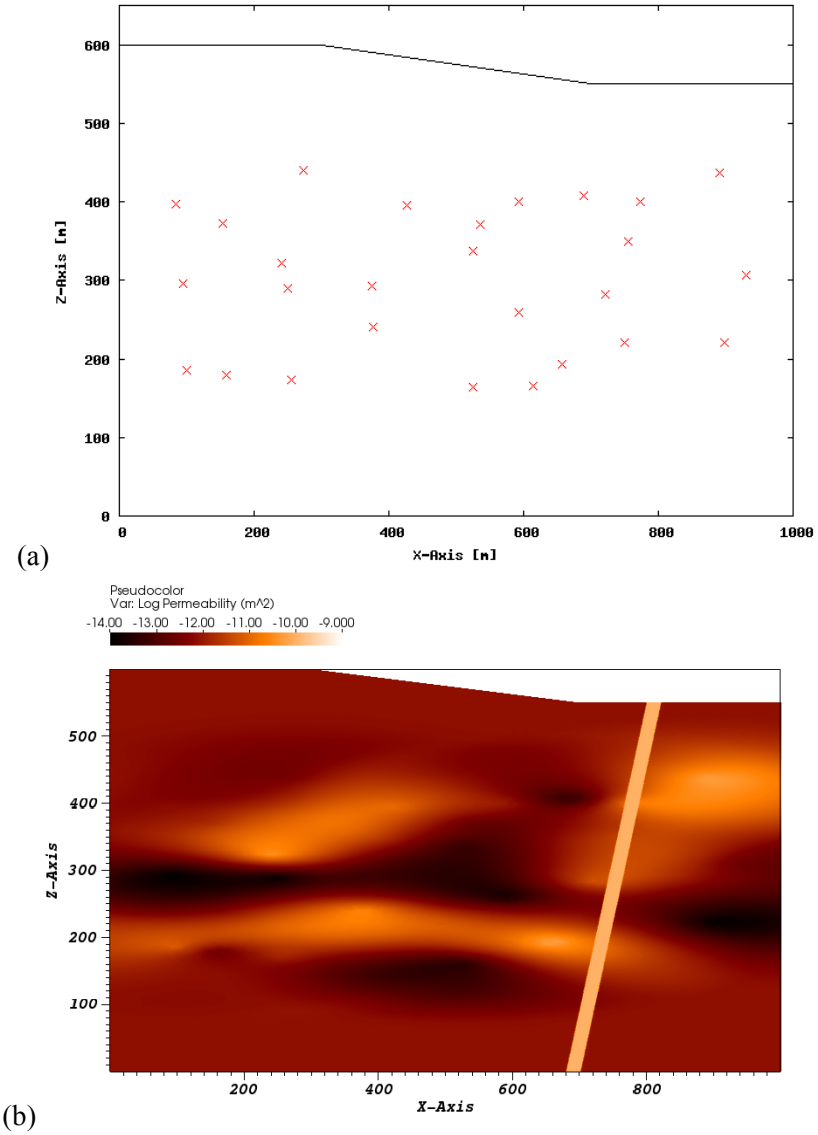


**Figure 2-3: 2D slice of (a) locations of conditioning points and (b) 'true' permeability field.**

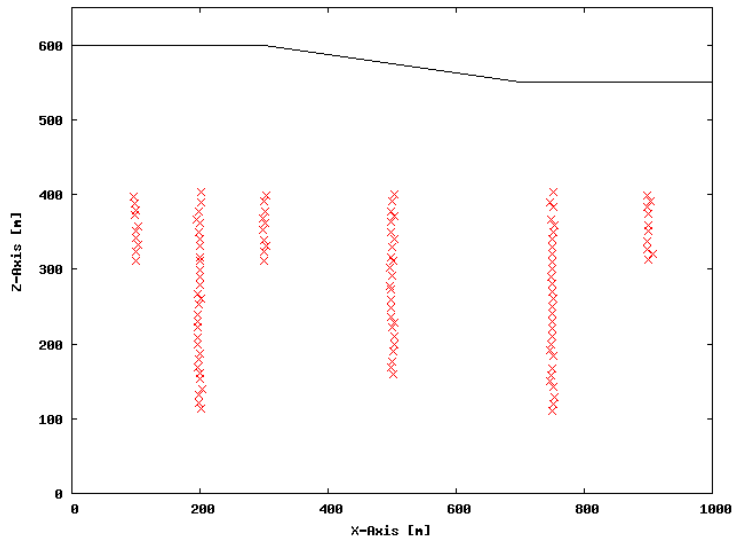


**Figure 2-4. Locations where steady state hydraulic heads are observed.**

Steady-state hydraulic heads were simulated using PFLOTRAN. Simulation run times were around 10-16 seconds on a single processor. While PFLOTRAN is a parallel code capable of utilizing multiple processors, the degrees of freedom in the current model did not warrant the use of this capability. In an actual application, it is expected that the model would be more complicated and the integrated assessment would benefit from parallel flow simulations.

As described in Section 1.2, a calibration-constrained uncertainty analysis followed by a sampling based uncertainty analysis was performed. In the demonstration, head observations from the synthetic site were used in a calibration-constrained uncertainty analysis to constrain the velocity fields, while a sampling-based uncertainty analysis was used to evaluate parametric uncertainties associated with radionuclide retention properties.

The following are the steps in the analysis

1. Perform NSMC on PFLOTRAN simulations to obtain 100 velocity fields constrained to head observations. The pilot point approach (RamaRao *et al.*, 1995) was used to constrain the heterogeneous permeability field.
2. Calculate flow paths from calibration-constrained velocity fields using Walkabout.
3. Perform LHS sampling of matrix retention parameters.
4. Use MARFA to calculate radionuclide transport using the calculated flow paths and sampled matrix retention parameters. The MARFA calculations were done in a way that integrated the NSMC results within MARFA. This was accomplished by weighting the source of each flow path by its generalized likelihood based on their objective function value from NSMC. This causes MARFA to preferentially release particles along flow paths with greater likelihood.
5. Postprocess the LHS to obtain histograms of cumulative breakthrough of radioactivity, maximum dose rate, and time to maximum dose rate at the ground surface.

### 2.2.2 Calibration Constrained Construction of Velocity Fields

NSMC is used here to obtain velocity fields constrained to the 115 hydraulic head observations (Figure 2-4) allowing the heterogeneous permeability field to vary using the pilot points approach (RamaRao *et al.*, 1995). The 27 conditioning points in Figure 2-3 (a) are used as the pilot points. The objective function is the sum-of-squared residuals expressed as

$$\min_{\Theta} \Phi(\Theta) = \sum_{i=1}^{N} r_i^2 \qquad (2\text{-}1)$$

where $\Phi(\Theta)$ is the objective function, $\Theta$ is a vector containing the model parameters (i.e. permeabilities at the pilot points), N is the number of measurements, and $r_i$ is the *i*-th model residual defined as $y_i - \hat{y}_i$, where $y_i$ and $\hat{y}_i$ are the *i*-th head measurement and simulated value from the PFLTRAN model, respectively.

NSMC involved the following steps:

1. Obtain a calibrated model (using singular value decomposition (SVD) if the number of parameters is large);
2. Compute sensitivities of the calibrated model;
3. Based on sensitivities from the calibrated model, determine the calibration space and null sub-space of the parameter space;
4. Generate samples within the null space;
5. Recalibrate samples using PEST's SVD-Assist with sensitivities from step 2.

The initial calibration of the PFLOTRAN model was performed using Parallel PEST (PPEST) with 9 processors and required 1075 model calls. PPEST reduced the objective function from 0.258 to $8.33 \times 10^{-4}$. The evolution of the minimization of the objective function during the calibration is presented in Figure 2-5.

Using the parameter sensitivities of the calibrated model, a set of 100 calibration-constrained velocity fields is generated. This is accomplished using PEST by creating 100 parameter sets with values fixed in the calibration solution space (i.e. parameter combinations that influence the calibration), but with random values in the null space (i.e. parameter combinations that do not influence the calibration). If these parameter sets are no longer in calibration, calibration with SVD-Assist is performed with the existing calibrated parameter sensitivities to recalibrate parameters spanning the calibration solution space while retaining the random values in the null space. This step uses existing sensitivities in a "superparameter" approach, and usually requires a small number of optimization iterations per recalibration. Figure 2-6 shows objective function values for the samples before and after recalibration.

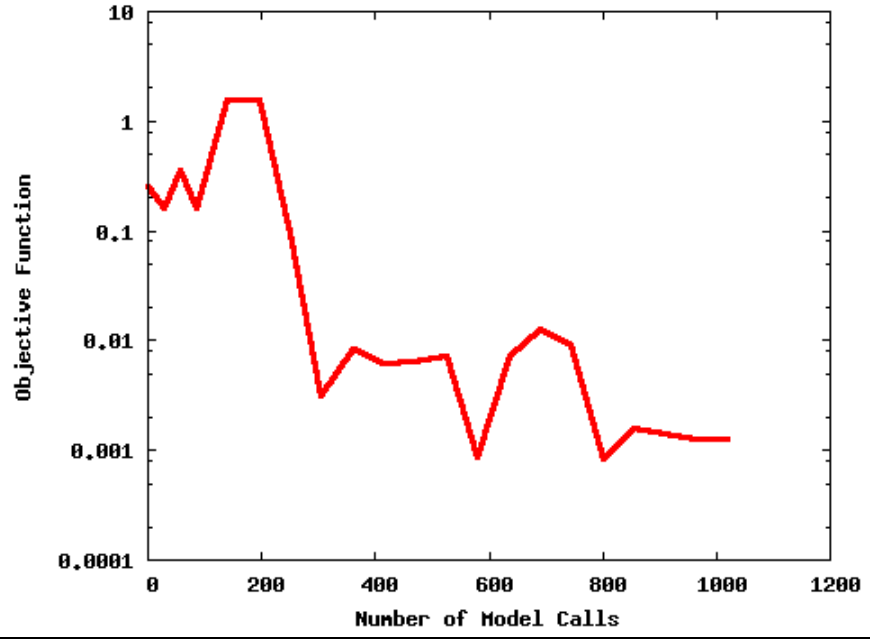


**Figure 2-5. Objective function as a function of the number of PFLOTRAN model calls during the initial calibration of the model.**

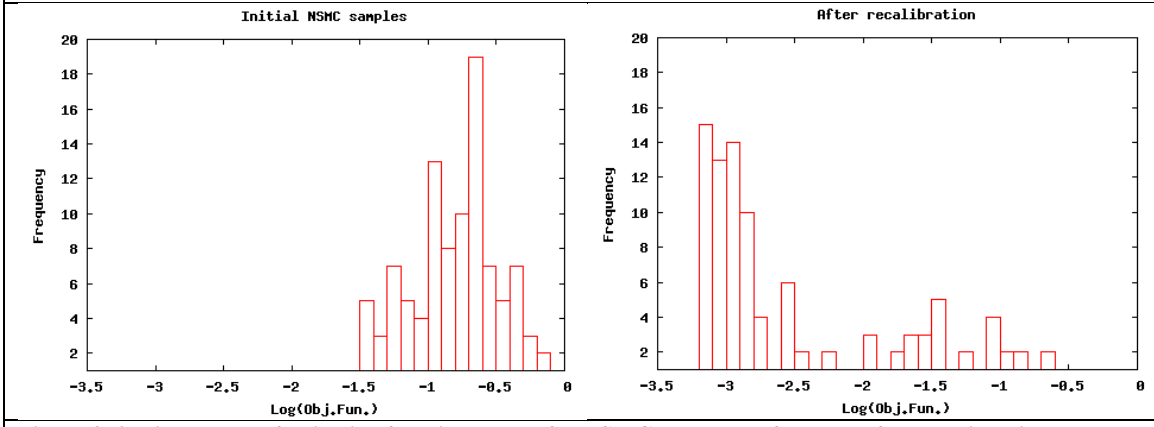


**Figure 2-6. Histograms of objective function values for NSMC samples before and after recalibration**

### 2.2.3 Calculation of Flow Paths

Flow paths were calculated from 20 locations within the repository to the point where they exit the model. The locations within the repository are selected along a horizontal line spanning the length of the repository and separated by 10 m. The flow paths for the 'true' heterogeneity are plotted over the 'true' permeability field in Figure 2-7.

Figure 2-8 presents the permeability field and flow paths for 4 of the 100 NSMC samples. It is apparent that the permeability fields and flow paths can have significant differences among calibration-constrained samples. Figure 2-9 plots the flow paths from all the NSMC samples in the same figure over the 'true' permeability field. From inspecting Figure 2-9, it is apparent that the flow paths are controlled by some of the features of the 'true' permeability field, i.e. the low permeability zone that runs horizontally around z=300 m. In Figure 2-8, it can be seen that this low permeability zone is present to some extent in the 4 realizations presented. Features of the permeability field that are deeper (lower z values) are less well

represented throughout the NSMC samples due to the lack of pilot points and head observations at these depths.

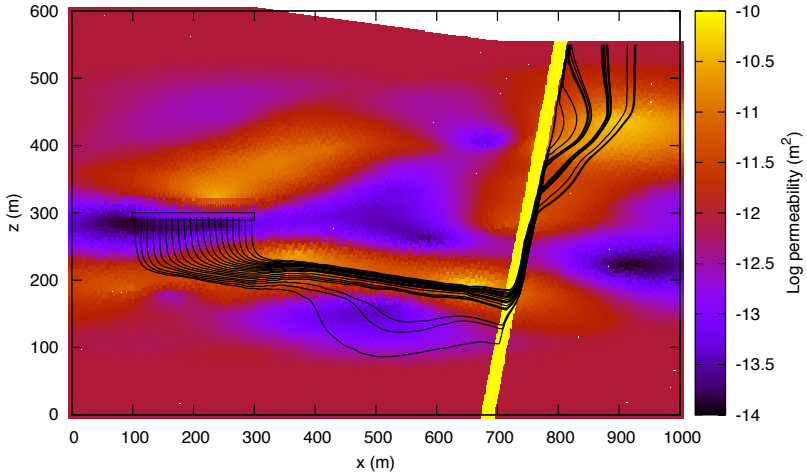


**Figure 2-7. Simulated flow paths from the repository to the ground surface for the 'true' model plotted as lines over the 'true' permeability field.**

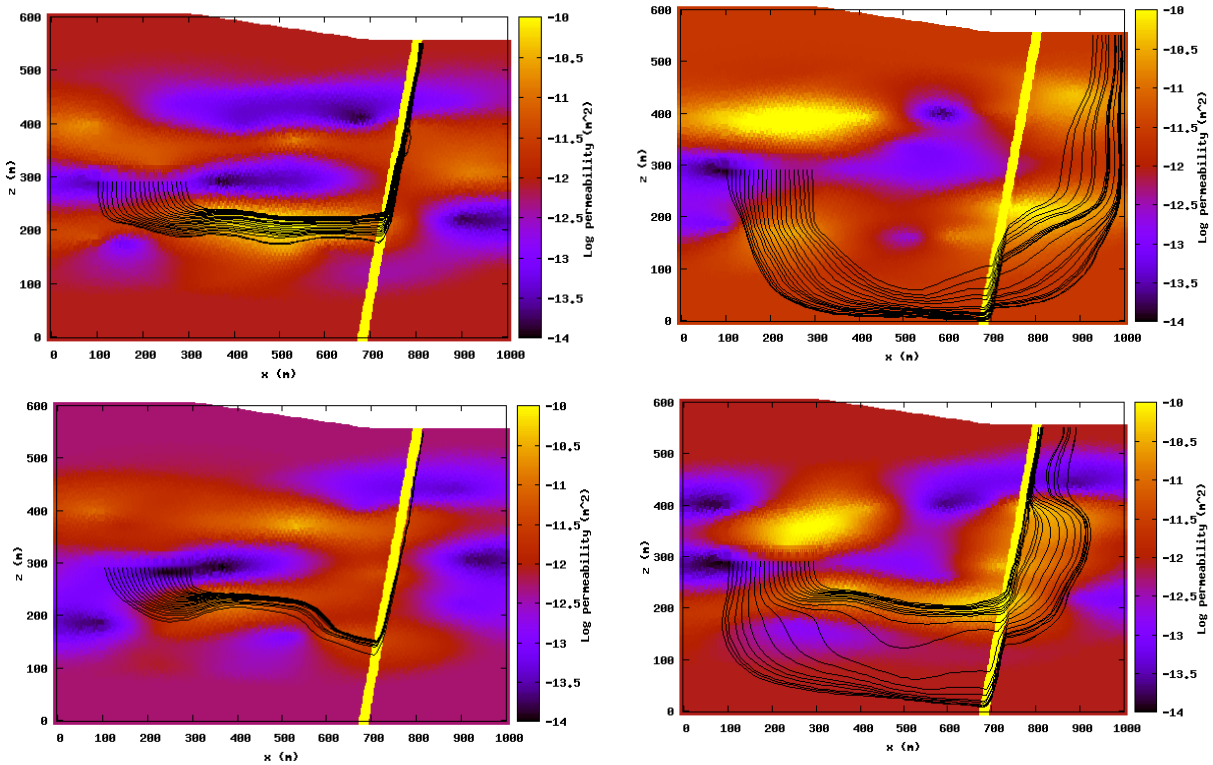


**Figure 2-8. Four realizations of permeability fields and associated flow paths. Each realization is consistent with the available hydraulic head and permeability measurements.**

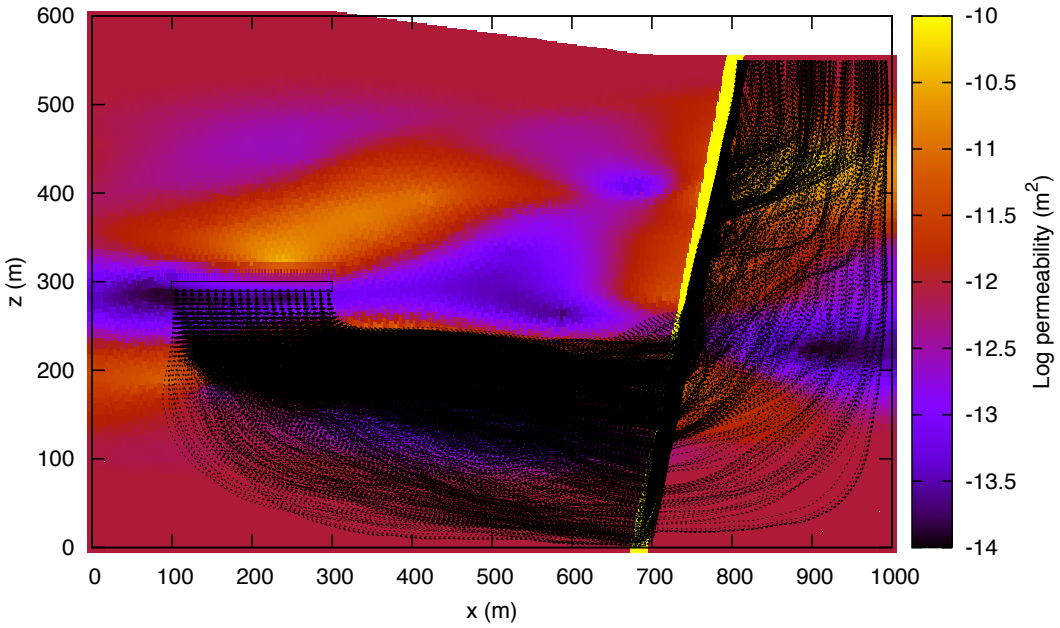


**Figure 2-9. Flow paths associated with 100 calibration-constrained samples of the uncertain permeability field plotted over the 'true' permeability field. Each flow path is consistent with available hydraulic head and permeability measurements.**

### 2.2.4 Radionuclide Transport

Breakthrough curves are computed by sampling the computed flow paths and retention properties. Sampling of flow paths is performed using the MARFA computer code (Painter and Mancillas, 2013), which models the transport of radionuclides along the computed flow paths. The radionuclide source associated with each flow path is weighted by its likelihood using a generalized likelihood (Beven and Binley, 1992) as

$$L=(\Phi^2)^{-N} \qquad (2\text{-}2)$$

where N is a user-specified parameter controlling the manner in which likelihoods are distributed across flow paths. If N=0, every flow path will have equal likelihood, while N→∞ will apply non-zero likelihood only to the flow path with the smallest Φ (i.e. best fit). N = 1.5 was selected here. The source for each flow path is calculated as

$$S_{0,i} = S_0 \frac{L_i}{\sum_{j=1}^{n} L_j} \qquad (2\text{-}3)$$

where $i$ is a flow path index, $S_0$ is the total source of radionuclides released from the EBS in mol/y and $n$ is the number of flow paths. Retention properties are sampled by LHS and used in independent runs of MARFA.

It was assumed that 1.0 mol/y of $^{237}$Np is released from the repository for a 1 year duration. We consider the Neptunium series through $^{229}$Th as $^{237}\mathrm{Np} \rightarrow {}^{233}\mathrm{Pa} \rightarrow {}^{233}\mathrm{U} \rightarrow {}^{229}\mathrm{Th}$. Given the relatively short half-life of $^{233}$Pa, it was ignored in the decay chain. Therefore, the decay chain $^{237}\mathrm{Np} \rightarrow {}^{233}\mathrm{U} \rightarrow {}^{229}\mathrm{Th}$ was modeled using decay constants of $3.2 \times 10^{-7}$ y$^{-1}$, $4.4 \times 10^{-6}$ y$^{-1}$, and $9.5 \times 10^{-5}$ y$^{-1}$, respectively.

Tables 2-1 and 2-2 contain the fixed and LHS sampled limited diffusion retention model rock properties. PyMADS was used to generate 100 samples from the retention properties defined in Table 2-1 and execute the MARFA runs concurrently.

Model results are presented as histograms of the cumulative radioactivity to reach the ground surface at 1 million years (Figure 2-10), the maximum dose rate at the ground surface (Figure 2-11), and the time of the maximum dose rate (Figure 2-12). This example is for demonstration purposes only. The dosages and times are not meant to be representative of a general or specific situation. The purpose of this synthetic example is to demonstrate the steps that could be taken for the assessment of a specific site.

**Table 2-1. Fixed retention properties**

| Parameter | Value |
|---|---|
| $\varrho_m$ [kg/m$^3$] | 2700 |
| $\Delta$ [m] | 2.0 |
| $k_a$ | 0 |
| $\alpha$ | 0 |
| $b$[m] | 0.0001 |

**Table 2-2. Sampled retention properties**

| Parameter | Distribution |
|---|---|
| $\Theta$ [–] | Uniform between $1\times10^{-3}$ and $2.5\times10^{-3}$ |
| $D_{eff}$[m$^2$/y] | Lognormal; mean= $2.0\times10^{-14}$, standard deviation= $1.6\times10^{-14}$ |
| $K_{d,Np}$ [m$^3$/kg] | Lognormal; mean=5.2 $\times10^{-2}$, standard deviation= $1.8\times10^{-1}$ |
| $K_{d,U}$ [m$^3$/kg] | Lognormal; mean=5.2 $\times10^{-2}$, standard deviation= $1.8\times10^{-1}$ |
| $K_{d,Th}$ [m$^3$/kg] | Lognormal; mean=5.2 $\times10^{-2}$, standard deviation= $1.8\times10^{-1}$ |

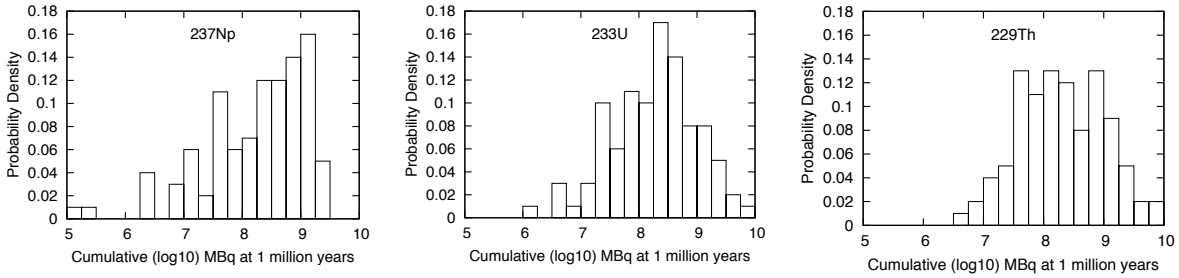


**Figure 2-10. Cumulative breakthrough of radioactivity at the ground surface at 1 million years.**

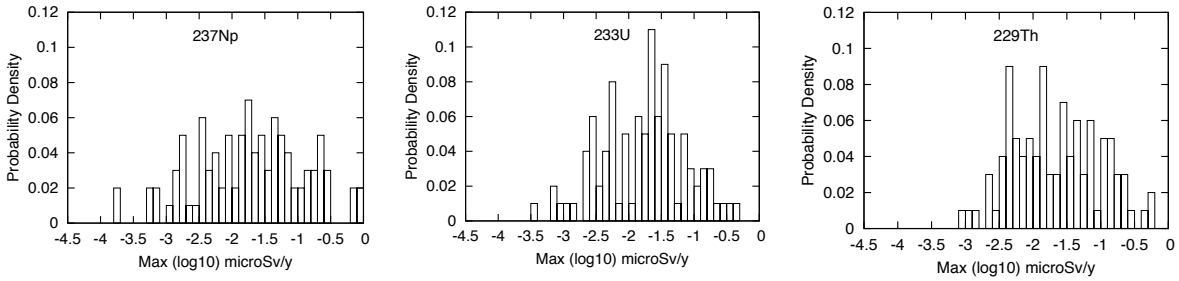


**Figure 2-11. Maximum dose rate at the ground surface.**

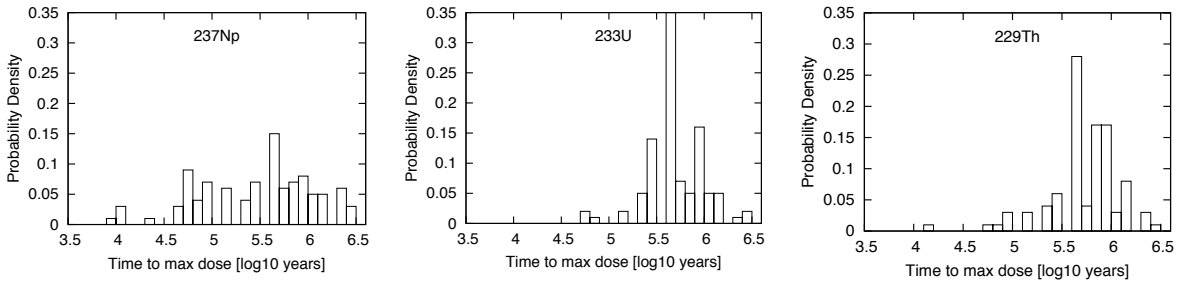


**Figure 2-12. Time of maximum dose rate at the ground surface.**

## 2.3 Summary

In summary, a workflow integrating parallel flow simulations with highly efficient transport modeling software in an uncertainty quantification framework was demonstrated on a generic granite repository example with characteristics similar to typical sites. Novel aspects of the work include calibration-constrained uncertainty analysis to produce realizations of permeability fields that are consistent with available hydraulic head measurements, the use multiple levels of parallelism combining concurrent simulations for uncertainty assessment with parallel flow simulations, and highly efficient particle methods specifically designed for integrated assessments. The framework or variants are expected to have wide applicability in analyses of natural system barriers. In addition, the framework can easily be extended to total system performance analysis by including appropriate process resolving software to represent engineered barrier systems and radionuclide transport in the surface ecological system.

**Acknowledgments:** The authors are grateful to Ethan Coon for careful review of this manuscript.

## 2.4 References

Beven, K., Binley, A., 1992. The future of distributed models: model calibration and uncertainty prediction. *Hydrological processes* **6**(3), pp. 279–298.

Campbell, J.E., Cranwell, R.M., 1988. Performance assessment of radioactive waste repositories. *Science*, **239**(18 March), pp. 1389–1392.

Coelho F. et al., bayesian-inference: Python package for object-oriented bayesian inference, http://code.google.com/p/bayesian-inference/.

Doherty, J., Brebber, L., Whyte, P., 1994. Pest. *Watermark Computing, Corinda, Australia*.

Ewing, R.C., Tierney, M.S., Konikow, L.F., Rechard, R.P., 1999. Performance assessments of nuclear waste repositories: A dialogue on their value and limitations. *Risk Analysis* **19**(5), pp. 933–958.

Gallegos, D.P., Bonano, E.J., 1993. Consideration of uncertainty in the performance assessment of radioactive waste disposal from an international regulatory perspective. *Reliability Engineering and System Safety*, **42**(2-3), pp. 111–123.

Harp, D.R., Painter, S.L., 2012. Report on Integrated Tool Development for Natural System Evaluation: LANL Input. Los Alamos National Laboratory, LA-UR-12-24251.

LaGriT, 2013. LaGriT project web site. *lagrit.lanl.gov*

Lichtner, P.C., Hammond, G.E., Lu, C., Karra, S., Bisht, G., Andre, B., Mills, R., Kumar, J., 2013 *PFLOTRAN User Manual: A Massively Parallel Reactive Flow and Transport Model for Describing Surface and Subsurface Processes*. LANL report LA-UR-06-7048, Los Alamos National Laboratory, Los Alamos, New Mexico.

Nuclear Energy Agency, 1990. Disposal of High-Level Radioactive Wastes: Radiation Protection and Safety Criteria. In: NEA Workshop, Paris, 5-7 November 1990. NEA, Organisation for Economic Co-Operation and Development, Paris, 1991, Paris.

Painter, S., Mancillas, J., 2013. *MARFA User's Manual: Migration Analysis of Radionuclides in the Far Field*. Posiva Working Report 2013-01, Posiva Oy, Helsinki, Finland.

RamaRao, B. S., LaVenue, A. M., De Marsily, G., and Marietta, M. G., 1995. Pilot point methodology for automated calibration of an ensemble of conditionally simulated transmissivity fields: 1. Theory and computational experiments. *Water Resources Research*, **31**(3), 475-493.

Tonkin, M., Doherty, J., 2009. Calibration-constrained Monte Carlo analysis of highly parameterized models using subspace techniques. *Water Resources Research*, **45**(12), W00B10.

Vanovschi, V., 2010. *Parallel Python Software*. http://www.parallelpython.com.

Vesselinov, V., *et al.*, 2013. MADS project web site. *mads.lanl.gov*.

# 3. USE OF COUPLED DAKOTA-PFLOTRAN TO MODEL RADIONUCLIDE TRANSPORT IN THE FAR FIELD OF A GENERIC SALT REPOSITORY

The present study is a continuation of the integrated tool development work documented in Wang et al (2012, Section 3). The previous work used coupled DAKOTA-FEHM codes to model flow and transport in the far-field of a generic salt repository. In this study the flow and transport code FEHM (Zyvoloski, 2007; Zyvoloski, et al. 1997) was replaced by PFLOTRAN (Hammond et al. 2011; Lichtner and Hammond, 2012) to include different capabilities and to align the integrated tool development study with that of the Generic Disposal System Modeling (GDSM). Features of PFLOTRAN of interest to this study include capabilities such as massively parallel flow and transport computation, and solution of transport by directly solving advection-diffusion equations. Development of DAKOTA-PFLOTRAN coupled codes for the Generic Disposal System Modeling (GDSM) was utilized for this study.

The performance assessment concept described in Wang et al. (2012, Section 3) is still applicable to the present study. The integrated tool development is based on the performance assessment (PA) and prototype framework first reported by Wang et al. (2010). For tool development a prototype framework is developed with applications to flow and transport in the far field of a geologic repository in salt.

The general PA concept is briefly summarized here for convenience. The flow chart for an enhanced PA system is shown in Figure 3-1. The forward model components in the flow chart represent the steps taken in a typical existing PA methodology. The PA starts with Features, Events, and Processes (FEPs) evaluation, through which potentially important FEPs are identified for inclusion for further PA analysis. The next step of the forward PA analysis is to develop appropriate computational models for the performance scenarios defined by the selected FEPs, followed by input parameter evaluation. The model input parameter values and their uncertainty distributions are constrained based on field observations and laboratory experimental data. The whole cycle of a PA analysis is then completed by uncertainty quantification and sensitivity analysis, typically performed using multiple Monte Carlo simulations. The PA process is generally iterative. The new concept extends the existing PA methodology by adding the inverse model components, as shown in Figure 3-1. These inverse components provide necessary tools for optimization of long-term system performance, process optimization, as well as updating of parameter estimates as new data are obtained. To fulfill these new functionalities, the PA system must have a built-in optimization capability. The new PA framework includes a built-in optimization capability for model parameterization and monitoring system design.

## 3.1 Integrated Tool Set Up

The high-level new PA architecture that can be applied to total system analysis is shown in Figure 3-2. The system consists of three layers. The middle layer hosts detailed process models to capture important physics involved in a high-level radioactive waste disposal. The bottom layer provides all necessary data to support process model runs. These two layers are then wrapped by a PA driver that is able to couple different process models, direct Monte-Carlo simulations, and assist PA analysis. In order for the PA system to be able to do inverse modeling, the PA driver must have a built-in optimization capability. For this work DAKOTA was chosen to be the PA driver. DAKOTA (Design Analysis Kit for Optimization and Terascale Applications) is a powerful and versatile software toolkit that provides a flexible and extensible interface between simulation codes and iterative analysis methods used in large-scale systems engineering optimization, uncertainty quantification, and sensitivity analysis (Eldred et al, 2002). A full set of PA calculations imposes stringent requirements on process code performance. The process codes must be robust and fast enough to run multiple model simulations in a widely spanned model parameter space. For the work documented here, PFLOTRAN was used as the flow and transport simulator.

The DAKOTA-PFLOTRAN coupling allows for concurrent execution of code runs in a parallel computation mode when multiple CPUs are available. This scalable code execution mode allows fully coupled multiphase PFLOTRAN simulations with various levels of complexity to be completed in a reasonable amount of time.

As stated above the integrated tool development for far-field radionuclide transport was developed by wrapping the flow and transport reservoir simulator (PFLOTRAN) with the uncertainty quantification and optimization code (DAKOTA).

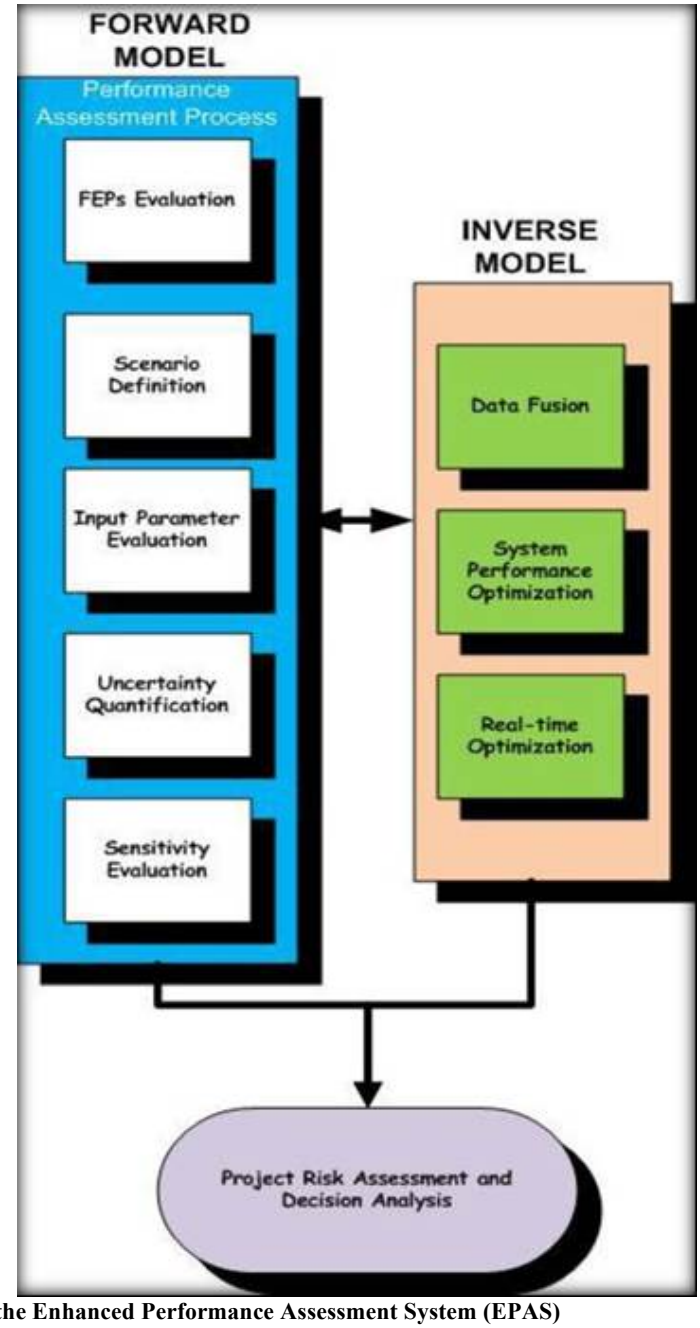


**Figure 3-1. Flow chart of the Enhanced Performance Assessment System (EPAS)**

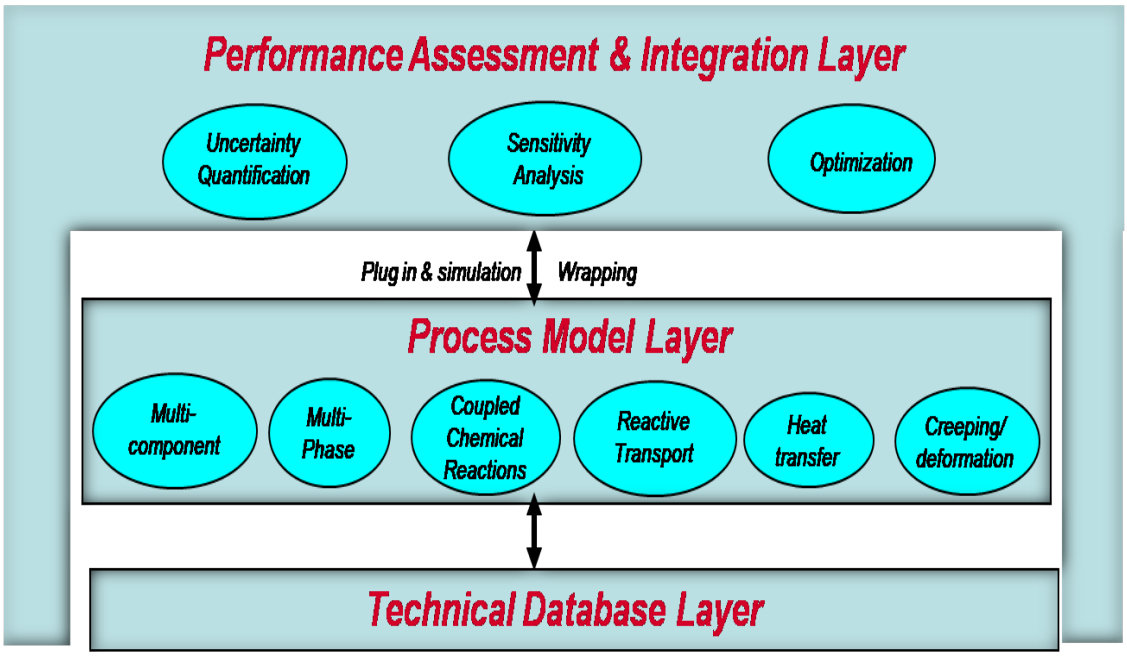


**Figure 3-2. An example of total performance assessment system architecture**

### 3.1.1 Description of the PFLOTRAN Flow and Transport Simulator

PFLOTRAN solves a system of generally nonlinear partial differential equations describing multiphase, multicomponent and multiscale reactive flow and transport in porous materials (Lichtner and Hammond, 2012). The code is designed to run on massively parallel computing architectures as well as workstations and laptops (Hammond et al., 2011). Parallelization is achieved through domain decomposition using the PETSc (Portable Extensible Toolkit for Scientific Computation) libraries for the parallelization framework (Balay et al., 1997). For this study PFLOTRAN has been used to model flow and transport in the far-field of a generic salt repository.

### 3.1.2 Description of DAKOTA

DAKOTA (Design Analysis Kit for Optimization and Terascale Applications) is a software toolkit that provides a flexible and extensible interface between simulation codes and iterative analysis methods used in large-scale systems engineering optimization, uncertainty quantification, and sensitivity analysis (Eldred et al, 2002). The DAKOTA toolkit can perform parameter optimization through the use of gradient and nongradient-based methods. It can also be used to conduct sensitivity analysis with the purpose of investigating variability in response to variations in model parameters using sampling methods such as Latin Hypercube Sampling (LHS), among others. Further capabilities of the toolkit include uncertainty quantification with sampling, analytic reliability, and stochastic finite element methods; and parameter estimation with nonlinear least squares methods. These capabilities may be used on their own or as components within system models. By employing object oriented design to implement abstractions of the key components required for iterative systems analyses, the DAKOTA toolkit provides a flexible and extensible problem-solving environment for design and performance analysis of computational models on high performance computers.

### 3.1.3 Wrapping PFLOTRAN with DAKOTA

Specific to this study, a DAKOTA based nondeterministic sampling algorithm is implemented for the new performance assessment framework. Figure 3-3 schematically depicts the overall scheme of how DAKOTA is coupled to PFLOTRAN. The overall sampling flow involves embedded PFLOTRAN functional evaluations within a DAKOTA run. First, a set of uncertain parameters with assigned probability distributions is specified in the DAKOTA input parameter file. A sample is drawn using Latin Hypercube sampling (LHS) internal to DAKOTA. The sample is processed by an input filter routine to transcribe each sample element, comprising a value for each uncertain parameter, into a formatted template file that is compatible with PFLOTRAN. After each sample element is executed, an output filter extracts the pertinent output values via an output filter routine and returns these to DAKOTA.

LHS is a stratified sampling method where the range of each variable to be sampled is divided into intervals of equal probability and a value is randomly sampled from each interval (Adams et al., 2010). Sampled values are randomly paired for different variables to form sample elements. Overall, LHS needs fewer samples relative to other random sampling methods (e.g., Monte Carlo) to obtain statistically stable estimates of mean values and has become widely used in uncertainty analysis. DAKOTA summarizes the statistical spread of the output observations at the completion of each DAKOTA run.

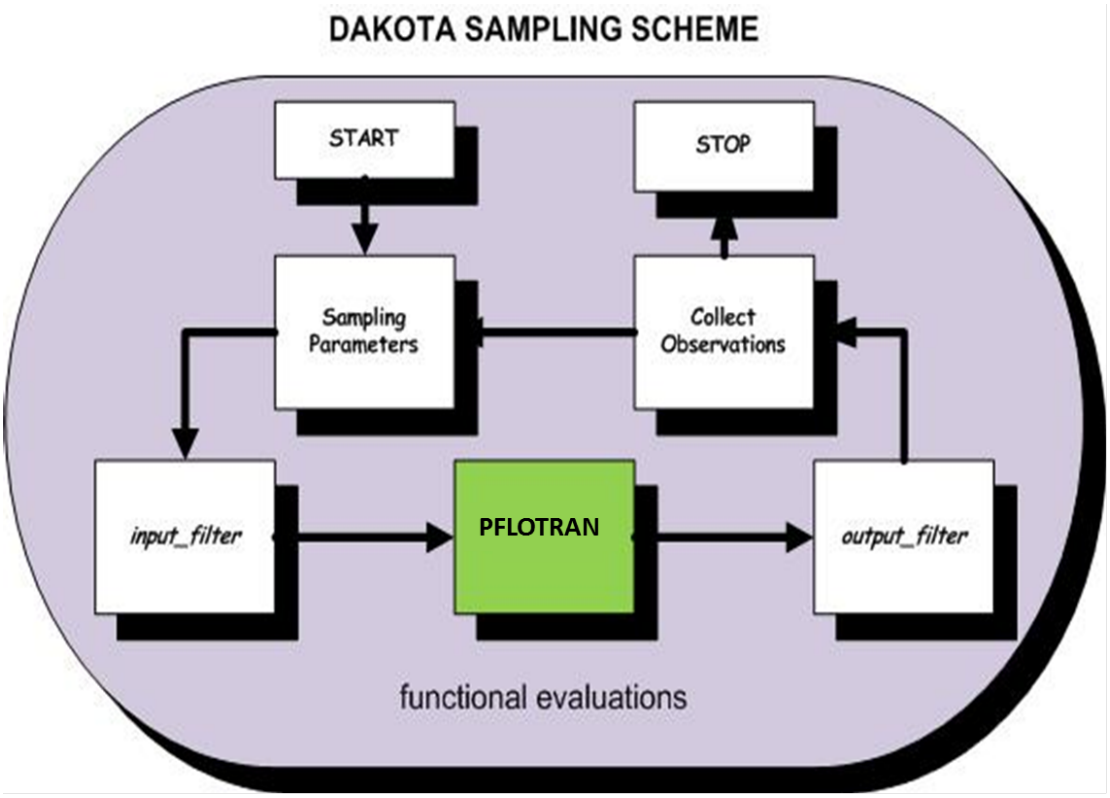


**Figure 3-3. Schematic diagram of DAKOTA-based PA framework**

### 3.1.4 Parallel Version of PFLOTRAN-DAKOTA

DAKOTA is designed to support large-scale simulations that can be computationally intensive. Different levels of parallelism are available in DAKOTA. In Wang et al. (2012, Section 3) a hybrid parallelism was used where DAKOTA was run in parallel, while directing serial runs of the flow and transport code FEHM. For the new framework a nested parallelism, where both DAKOTA and PFLOTRAN are run in

parallel is used. Figure 1.4 shows how the flow of information works in the nested parallelism implementation. Extraction scripts embedded in the DAKOTA simulation script were also developed for the extraction of PFLOTRAN outputs in each code run.

Specification of asynchronous concurrency within DAKOTA provides a level of parallelism at functional evaluation level. A number of concurrent parallel PFLOTRAN jobs can be executed at any given time as long as the computational CPUs are available. This level of parallelism essentially shortens the overall calculation cycle. Such coupling can further be refined and expanded to run in parallel on the high-performance computational clusters.

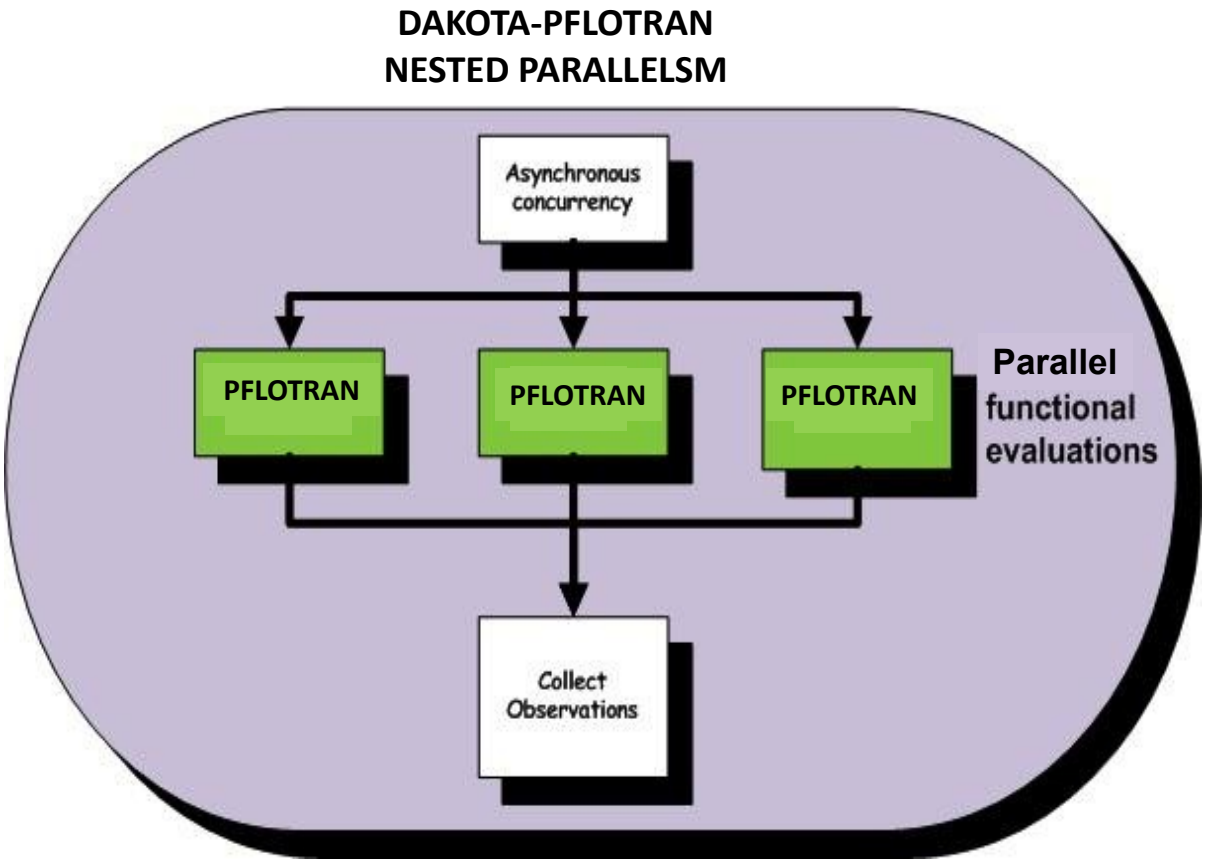


**Figure 3-4. Schematic diagram of nested parallelism**

## 3.2 Modeling of Flow and Transport in the Far Field of a Generic Salt Repository

For demonstration of the coupled DAKOTA-PFLOTRAN codes isothermal flow and transport simulations were conducted in the far field of a generic high-level nuclear waste repository in bedded salt, as was also done in Wang et al. (2012, Section 3). Although the system modeled is a dual-porosity fractured aquifer, a single porosity porous medium was assumed for the present study. Future simulations will include dual-porosity implementation. For this exercise the disturbed case scenario, where

radionuclides are transported upwards in a borehole from the repository to the transport domain is assumed. This allows a direct transport of radionuclides from the repository to the far field.

### 3.2.1 Flow Simulations

Transport in the far field of a generic repository is a function of groundwater flow represented by transmissivity fields. For this analysis groundwater flow data with generic transmissivity fields were used.

The far-field stratigraphic layer modeled in the present study has a total thickness of 7.75 m, which includes a permeable 4 m thick lower part. For groundwater flow calculations, the full 7.75 m thickness of the layer was used, while for transport purposes the thickness is reduced to 4.0 m to focus all flow through the lower, more permeable portion. In both flow and transport simulations the stratigraphic layer was modeled as a single porosity system. The flow domain covers an area of 28.4 km (east-west) by 30.7 km (north-south). Transmissivity fields were obtained for the flow domain for grid blocks of 100 m x 100 m x 7.75 m size. For transport calculations the domain used is a subregion of that used for the groundwater flow calculations, and covers an area of about 7.5 km by 5.4 km.

For this exercise flow and transport in the transport domain has been modeled. The geometry of the simulation domain is 7500 m x 5400 m by 4 m thickness. The mesh was generated internally by PFLOTRAN. The grid consists of a two-dimensional uniform mesh with 100 m x 100 m x 4 m grid blocks for a total of 4050 grid blocks (Figure 3-5). Permeability, horizontal anisotropy and head data (i.e. transmissivity fields) covering the transport domain were extracted from the larger groundwater flow domain. Perl scripts were used for extraction of data. For demonstration purposes only transmissivity fields for Realization 1 were used. PFLOTRAN forward steady-state groundwater flow simulation was first done using permeability, horizontal anisotropy fields and head boundary conditions at the boundary of the transport domain. For the simulation a fracture porosity of 0.01 was applied. Figures 1.6 to 1.10 show the x-permeability field, the y-permeability field, and steady state distributions of pressure, x-velocity and y-velocity as outputs of PFLOTRAN.

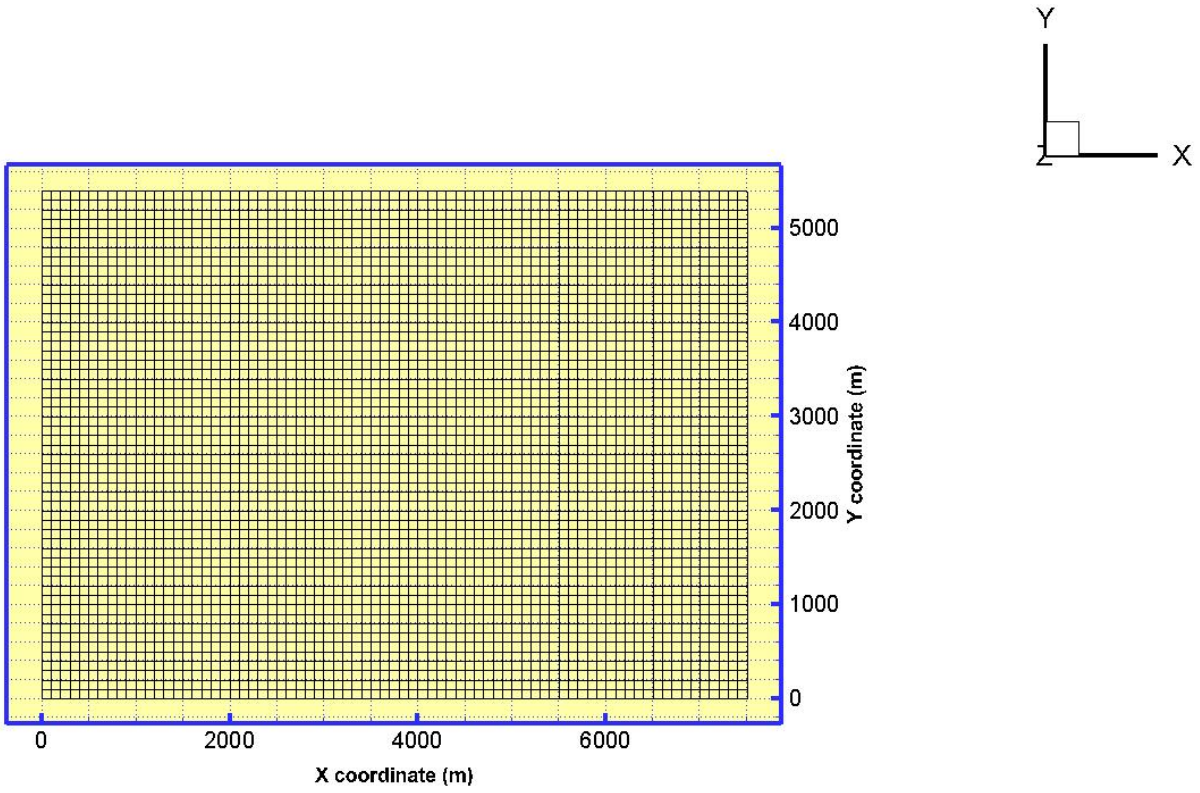


**Figure 3-5. Mesh representing the transport domain for Culebra Dolomite transport simulations (100m x 100m x 4 m blocks used)**

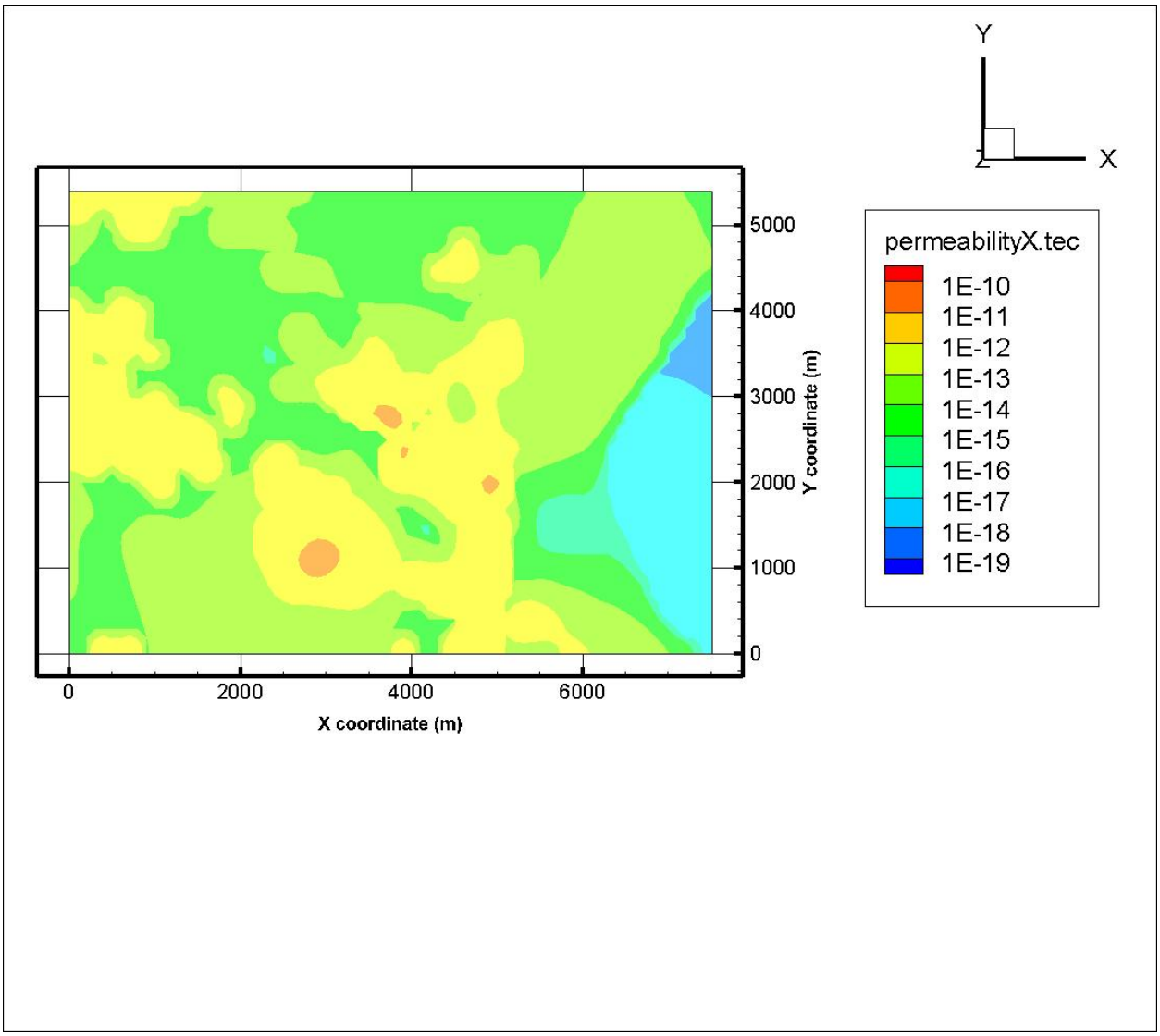


**Figure 3-6. Permeability field in the x-direction applied to the transport domain**

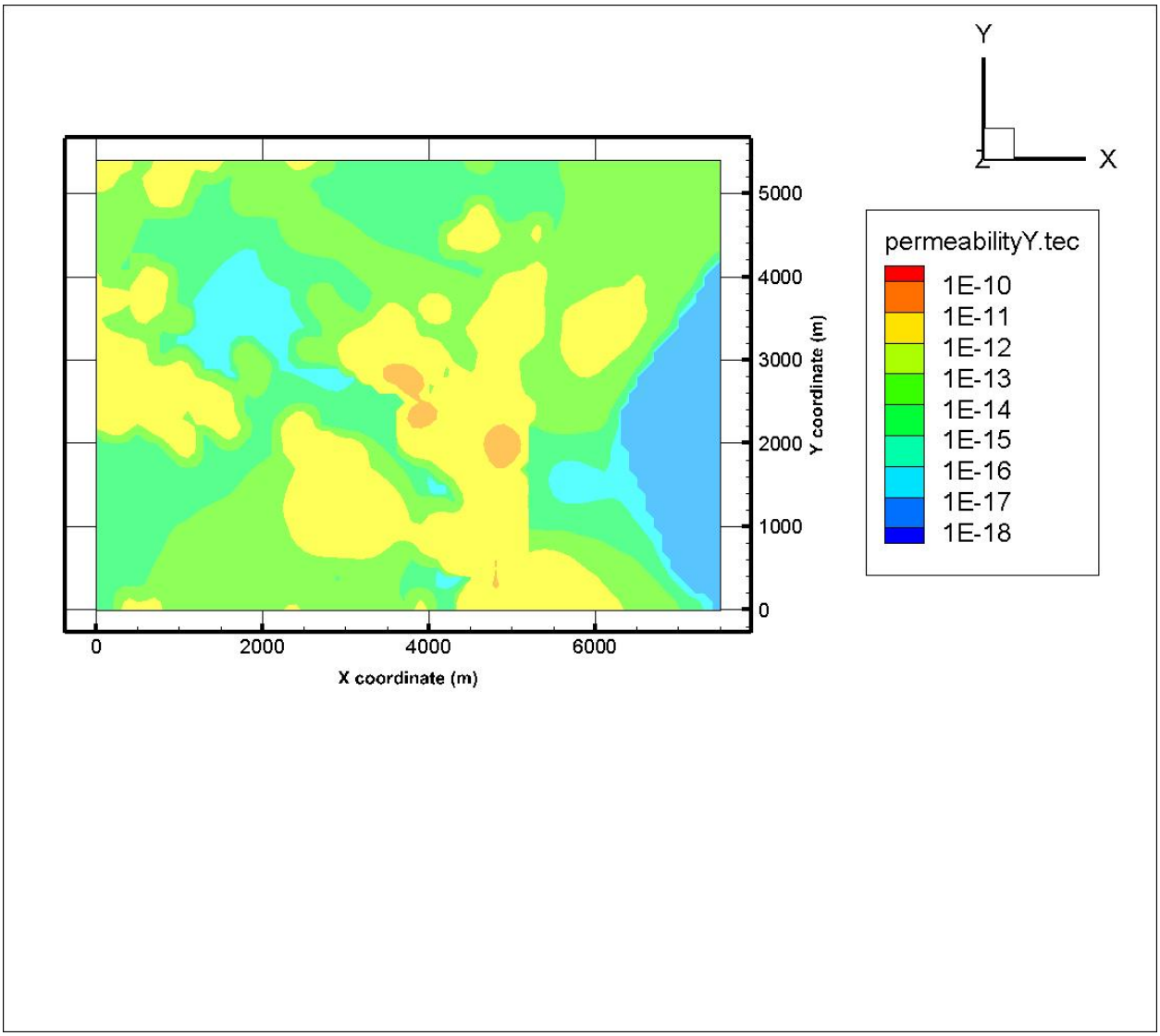


**Figure 3-7. Permeability field in the y-direction applied to the transport domain**

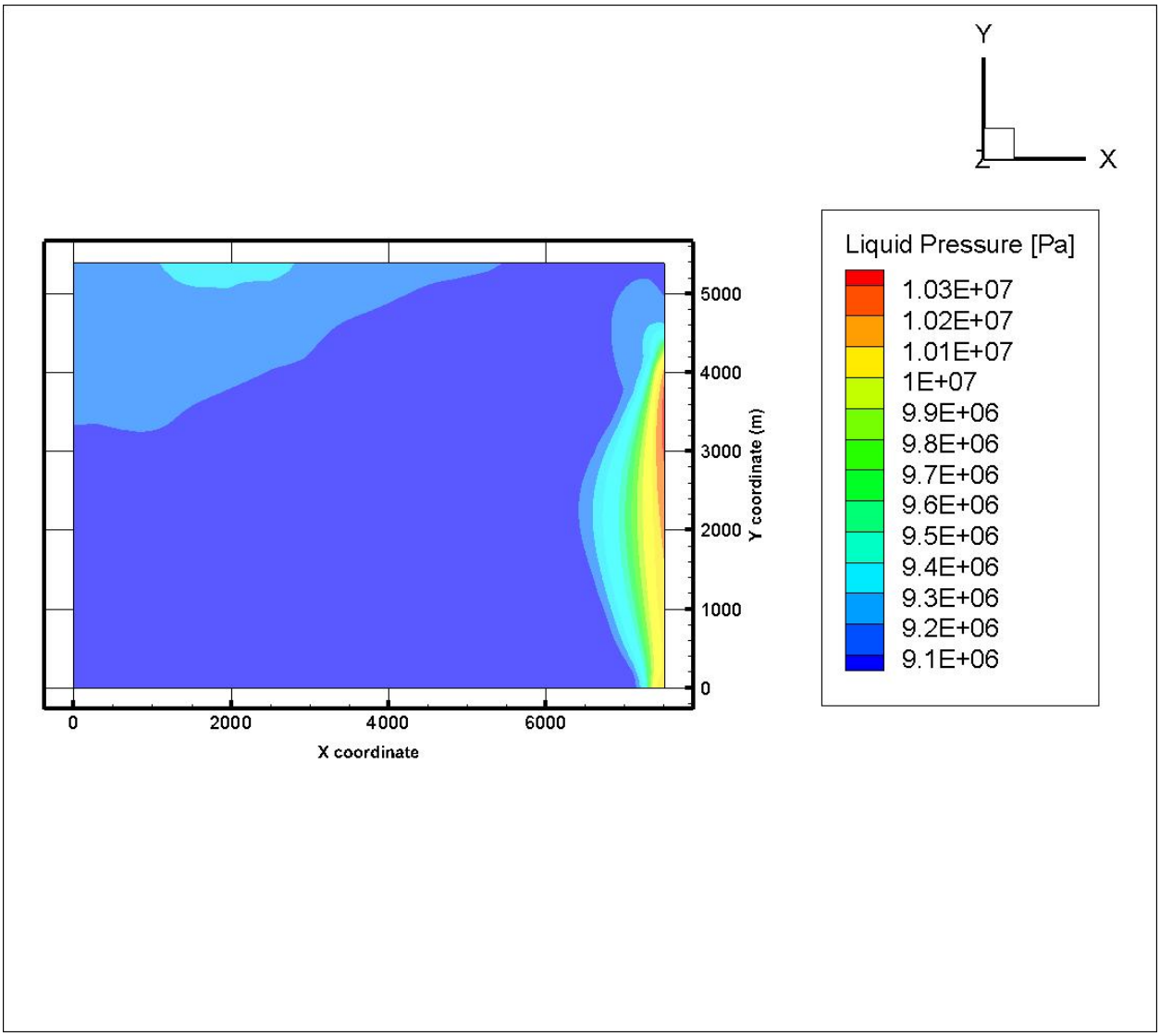


**Figure 3-8. Steady-state pressure distribution**

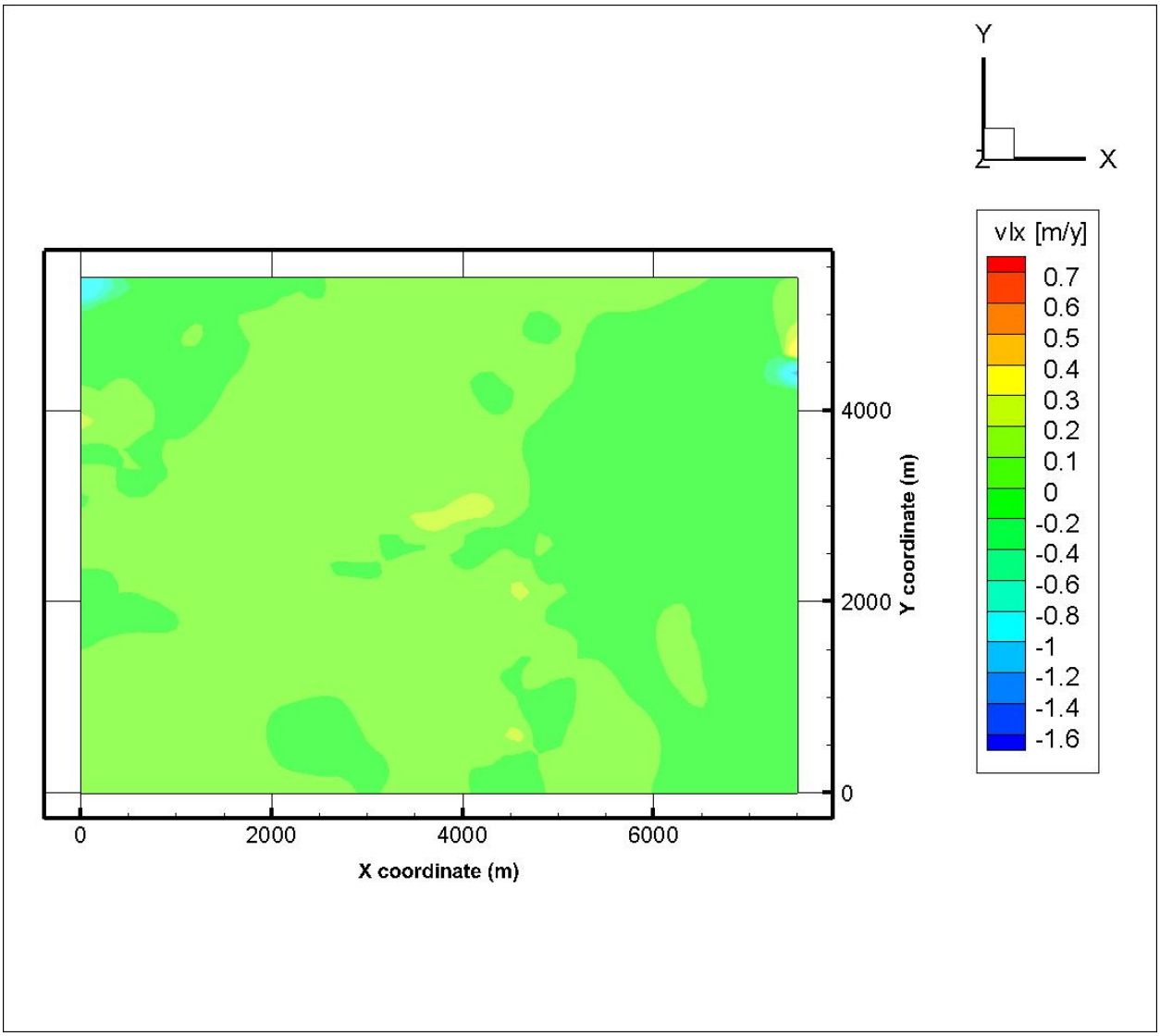


**Figure 3-9. Steady-state distribution of velocity in the x-direction**

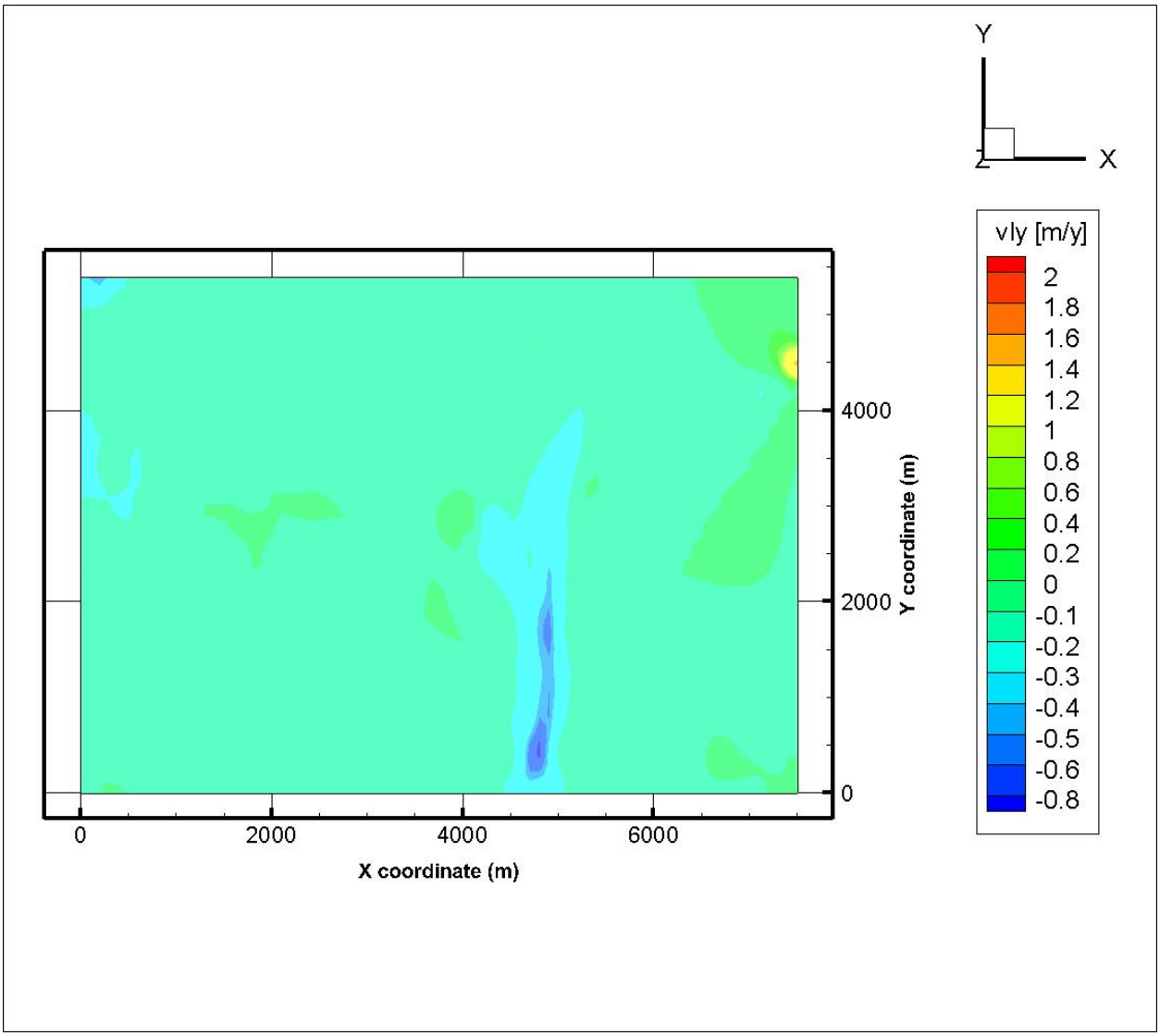


**Figure 3-10. Steady-state distribution of velocity in the y-direction**

## 3.2.2 Transport Simulations

### *3.2.2.1 Deterministic Simulations*

Modeling of transport started with PFLOTRAN-only simulations to obtain distributions of solute transport and breakthrough curves. In the current study transport was modeled by directly solving the advection-dispersion equations. Particle tracking was not used as was done in Wang et al. (2012, Section 3). For all transport simulations the steady state flow field was used as input. For the current study single-porosity transport modeling was assumed. For the deterministic simulations transport of a tracer was modeled. Tracer with a molality of 10 was injected at a release point located at x = 3100 m and y = 2000 m in the transport domain. The simulations did not include hydrodynamic dispersion and sorption. The results of the simulation are shown in Figures 3-11 to 3-14. Figures 3-11 to 3-13 show tracer distributions at different times. The tracer transport simulation did not include sorption, dispersion or decay, and thus movement of tracer to the domain boundary is relatively fast. The general transport direction is towards the southern boundary of the transport domain, which is an area of high transmissivity. The spread and quantity of tracer at the boundary depends on the released amount and simulation time. Figure 1.14 shows a breakthrough curve for relative mass of tracer at the boundary of the transport domain.

**Table 3-1. List of Input Parameters**

| **Parameter** | **Distribution Type** | **Parameter Value and Description** |
|---|---|---|
| Longitudinal dispersivity (m) | Constant | 0 |
| Transverse horizontal dispersivity (m) | Constant | 0 |
| Transverse vertical dispersivity (m) | Constant | 0 |
| Molecular diffusion coefficient ($m^2/s$) | Constant | 2.2E-09 |
| Material grain density ($kg/m^3$) | Constant | 2820 |
| Fracture porosity | Log-uniform | 1.0E-04 (min); 1.0E-02 (max) |
| *Kd for Radioelement (mL/g):* | | |
| I | Uniform | 0.0 (min); 1.0 (max) |
| Pu(IV) | Log-uniform | 0.5 (min); 1.0E+04 (max) |
| U(VI) | Log-uniform | 3.0E-02 (min); 2.0E+01 (max) |
| *Decay rate for Radioelement (1/s):* | | |
| I | Constant | 1.4E-15 |
| Pu(IV) | Constant | 5.0E-11 |
| U(VI) | Constant | 1.03E-14 |
| NOTE: Kd data for I is from Miller and Wang (2012); Decay rate for I is from GE Nuclear Energy (1989); decay rates of Pu(IV) and U(VI) were arbitrarily assigned for model demonstration. | | |

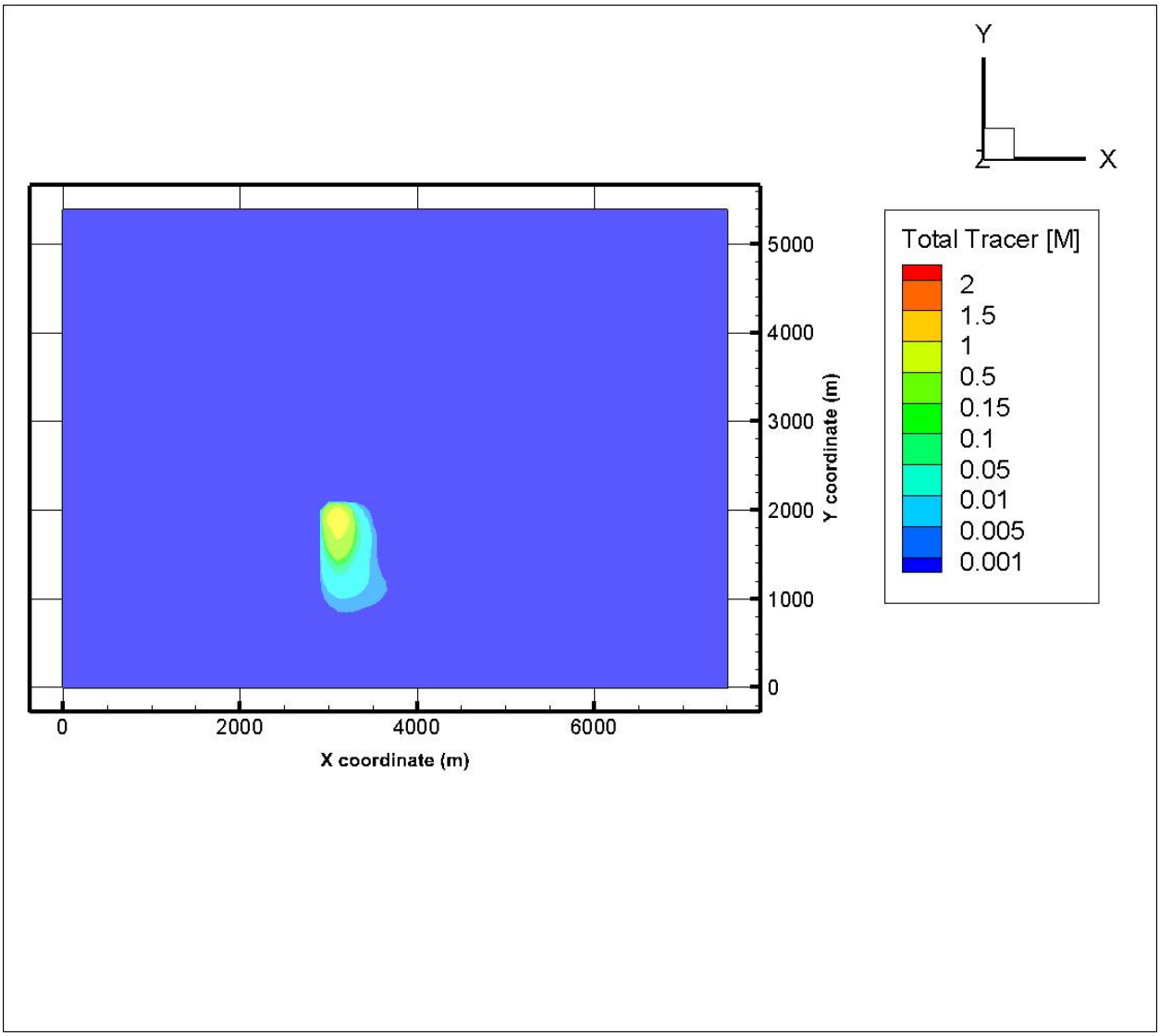


**Figure 3-11. Tracer distribution in the transport domain for the deterministic simulation case with no sorption or dispersion at 100 years simulation time (tracer placed at the source: x = 3100 m, y = 2000 m)**

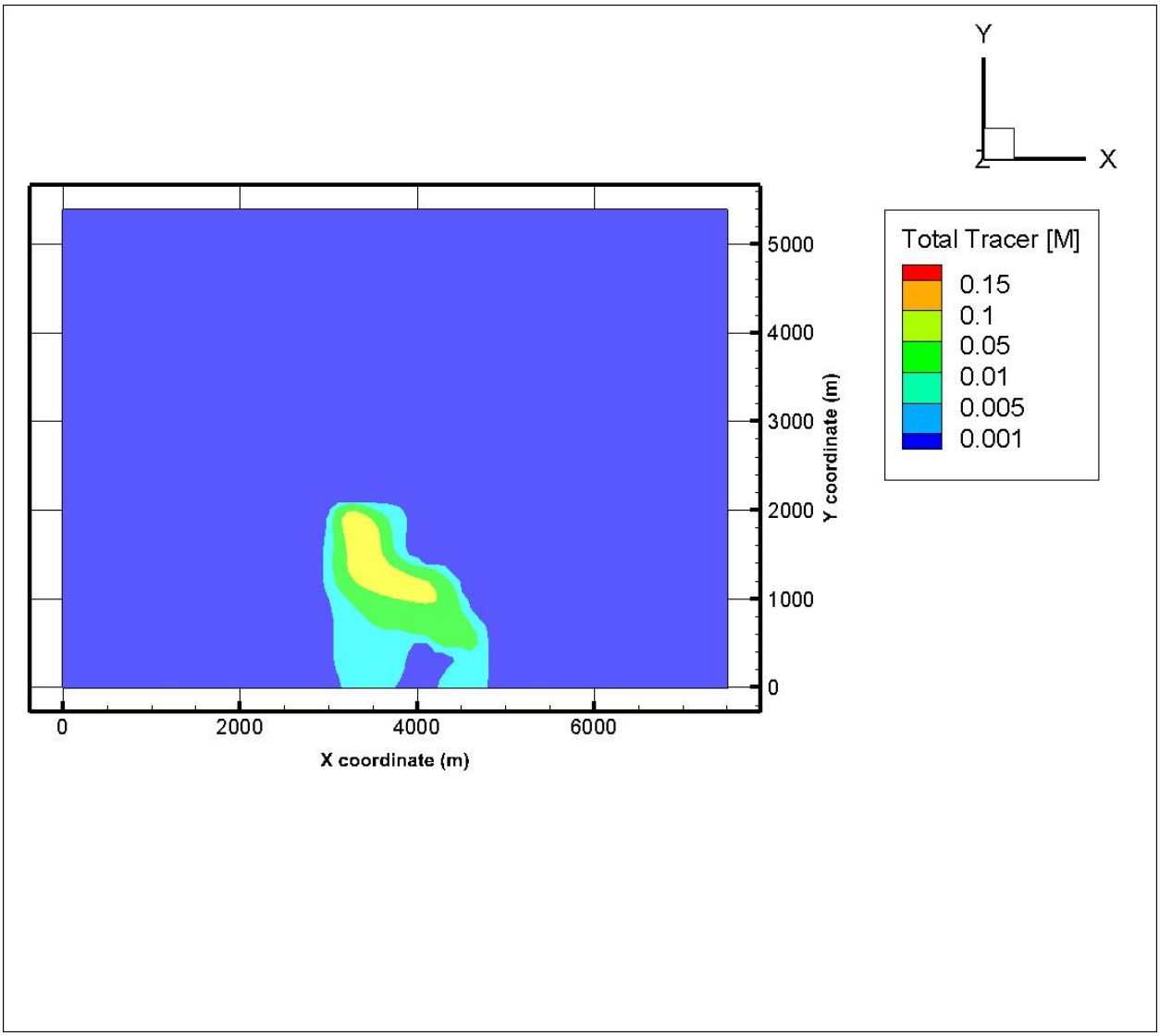


**Figure 3-12. Tracer distribution in the transport domain for the deterministic simulation case with no sorption or dispersion at 1000 years simulation time (tracer placed at the source: x = 3100 m, y = 2000 m)**

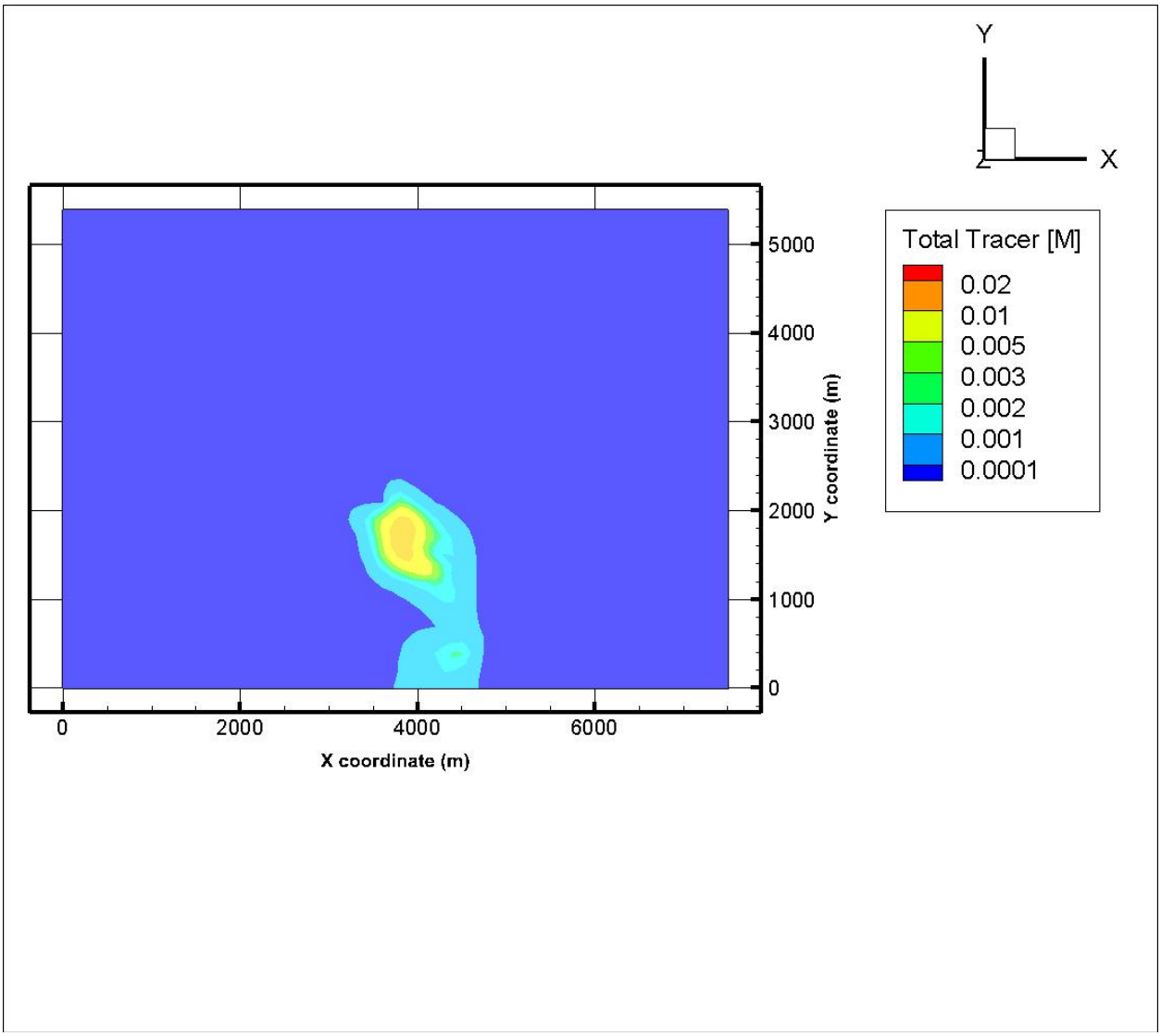


**Figure 3-13. Tracer distribution in the transport domain for the deterministic simulation case with no sorption or dispersion at 10,000 years simulation time (tracer placed at the source: x = 3100 m, y = 2000 m)**

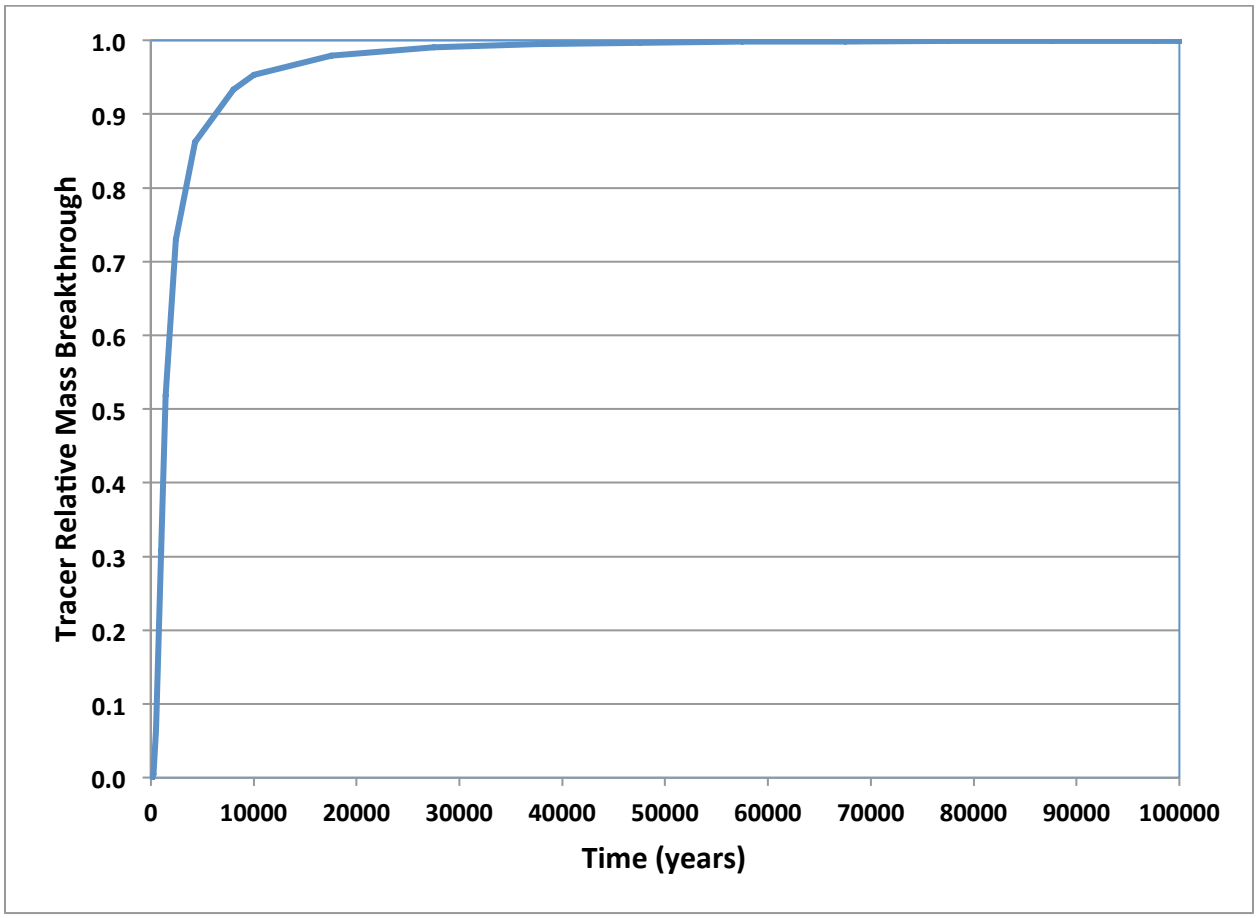


**Figure 3-14. Cumulative tracer relative mass breakthrough at the transport domain boundary for the deterministic simulation case with no sorption and dispersion (tracer placed at the source: x = 3100 m, y = 2000 m)**

#### 3.2.2.2 Probabilistic Simulations

Probabilistic simulations were conducted using the coupled DAKOTA-PFLOTRAN codes to simulate radionuclide transport from the release point to the transport domain boundary. Three radionuclides, Iodine, Pu(IV) and U(VI) were selected for the tool demonstration simulations, as was also done in Wang et al. (2012). The simulations include advection, diffusion, sorption, and decay processes. Parameter data in Table 1.1 were used for the simulations. The unit of Kd in PFLOTRAN is in kg water/$m^3$ bulk volume. Thus, the Kd data in Table 1.1 were converted to units used by PFLOTRAN. Derivation of the conversion equation is shown below.

**Determination of Kds for PFLOTRAN**

Typically Kd is given in mL/g. However, PFLOTRAN uses Kd in units of kg of water/$m^3$ bulk volume. To convert the typical Kd definition to the PFLOTRAN definition, we employ the definition of retardation.

Retardation is defined by the equation:

$$R = 1 + \frac{K_{dT} \cdot \rho_b}{\varphi} \qquad (3\text{-}1)$$

Where $K_{dT}$ = typical Kd definition (in $m^3$/kg)

$\rho_b$ = bulk density (kg/$m^3$)

$\phi$ = porosity

The PFLOTRAN definition of retardation is:

$$R = 1 + \frac{K_{dP}}{\varphi . \rho_w} \qquad (3\text{-}2)$$

Where $K_{dP}$ = PFLOTRAN Kd definition (kg of water/$m^3$ bulk volume)

$\rho_w$ = density of water (kg/$m^3$) = 1000

$\phi$ = porosity

Equating Equations (1) and (2) results in:

$$K_{dP} = K_{dT} . \rho_b . \rho_w \qquad (3\text{-}3)$$

Saturated bulk density is defined as:

$$\rho_b = \varphi \rho_w + (1 - \varphi)\rho_g \qquad (3\text{-}4)$$

Where $\rho_g$ = grain density (kg/$m^3$) = 2820

Substituting Equation (4) in Equation (3) results in an equation to determine Kd in PFLOTRAN units:

$$K_{dP} = K_{dT} . \rho_w \, [\varphi \rho_w + (1 - \varphi)\rho_g] \qquad (3\text{-}5)$$

Equation (5) can be simplified to obtain a direct conversion of Kds:

$$K_{dP} = K_{dT} . (1 - \varphi)\rho_g \qquad (3\text{-}6)$$

Note that $K_{dT}$ is given in mL/g. Equation (6) includes the conversion factor of $10^{-3}$ from mL/g to kg/$m^3$ and the density of water (1000 kg/$m^3$) which cancel each other out.

#### *3.2.2.3 Results of Probabilistic Simulations*

For this study the uncertain parameters include fracture porosity and Kds of the three selected radionuclides. DAKOTA generated 100 samples of each uncertain parameter, and parallel DAKOTA runs were setup to direct PFLOTRAN runs. PFLOTRAN was also run in parallel in two stages: first to obtain the steady state flow field, which is a function of fracture porosity, and second for transport simulation. For the steady state portion PFLOTRAN was run to a total time of $10^5$ years followed by a transport run to total time of $10^6$ years. PFLOTRAN and DAKOTA results for each radionuclide are described below. The results include scatter plots of cumulative relative mass at total time (i.e. the output) vs. each uncertain parameter (Figures 3-15 to 3-20), and tables of statistical data (Table 3-2). The tables of statistical data include Moment-based statistics for the output, 95% confidence intervals for each output**,** Simple Correlation Matrix among all inputs (i.e. uncertain parameters) and the output, Partial Correlation Matrix between input and the output, Simple Rank Correlation Matrix among all inputs and the output and Partial Rank Correlation Matrix between input and the output. The output is represented by three response functions. Response function 1 is the relative mass of Iodine at total time; response function 2 is the relative mass of Pu(IV) at total time; response function 3 is the relative mass of U(VI) at total time. Notations of the input and output parameters used in Table 1.2 are described below.

Kdi = Kd of Iodine

P1 = fracture porosity

Kdp = Kd of Pu(IV)

Kdu = Kd of U(VI)

response_fn_1 = relative mass of Iodine at total time

response_fn_1 = relative mass of Pu(IV) at total time

response_fn_1 = relative mass of U(VI) at total time

Figure 1.15 shows a scatter plot for Iodine with relative mass vs. Kd. The plot shows very high relative mass for all vectors at total time. This is likely due to the advection dominated transport in a single porosity medium combined with the low Iodine Kd range minimizing retardation. The simulation also used a low decay rate with reduced radioactive decay over the modeled total time. The influence of Iodine Kd on relative mass is observed at higher Kd values. Statistical data for Iodine transport is given in Table 1.2. The simple correlation matrix among all inputs and outputs shows a value of 0.094 for Iodine Kd indicating a weak correlation. The positive sign and the value may be a result of numerical errors.

Figure 1.16 shows a scatter plot for Pu(IV) with relative mass vs. Kd. In this plot the influence of Kd is more visible than in Figure 1.15. The figure shows a steep decline of relative mass with increase in Kd. The decline is also as a result of radioactive decay. The simulation used a much higher decay rate for PU(IV) compared to Iodine. The plot shows a transition at Kd of about 10.0 mL/g where sorption effectively retards advance of the Pu(IV) mass to the boundary. The simple correlation matrix among all inputs and outputs shows a value of -0.013 for Pu(IV) Kd. The negative sign is in line with the plot in Figure 1.16 showing inverse correlation.

Figure 1.17 shows a scatter plot for U(VI) with relative mass vs. Kd. In this plot the influence of Kd is more clearly visible. The figure shows a steep decline of relative mass with increase in Kd, as in Figure 1.16. The effect of radioactive decay is much less pronounced than for Pu(IV) because of the lower decay rate. The plot shows a transition at Kd of about 12.0 mL/g where sorption effectively retards advance of the Pu(IV) mass to the boundary. The simple correlation matrix among all inputs and outputs shows a value of -0.013 U(VI) Kd. The negative sign is in line with the plot in Figure 1.17 showing inverse correlation.

Figure 1.18 shows a scatter plot for Iodine with relative mass vs. fracture porosity. As in Figure 1.15 the plot shows very high relative mass for all vectors at total time. Any influence of fracture velocity on Iodine mass is not visible. The simple correlation matrix among all inputs and outputs shows a value of -1.000, indicating a strong inverse correlation.

Figure 1.19 shows a scatter plot for Pu(IV) with relative mass vs. fracture porosity. The plot does not seem to show a clearly defined relationship between relative mass and fracture porosity, although some trend is shown in the middle of the figure. The simple correlation matrix among all inputs and outputs shows a value of 0.014, indicating a weak direct correlation.

Figure 1.20 shows a scatter plot for U(VI) with relative mass vs. fracture porosity. As with Iodine and Pu(IV) the plot does not seem to show a clearly defined relationship between relative mass and fracture porosity. The simple correlation matrix among all inputs and outputs shows a value of -1.000, indicating a strong inverse correlation.

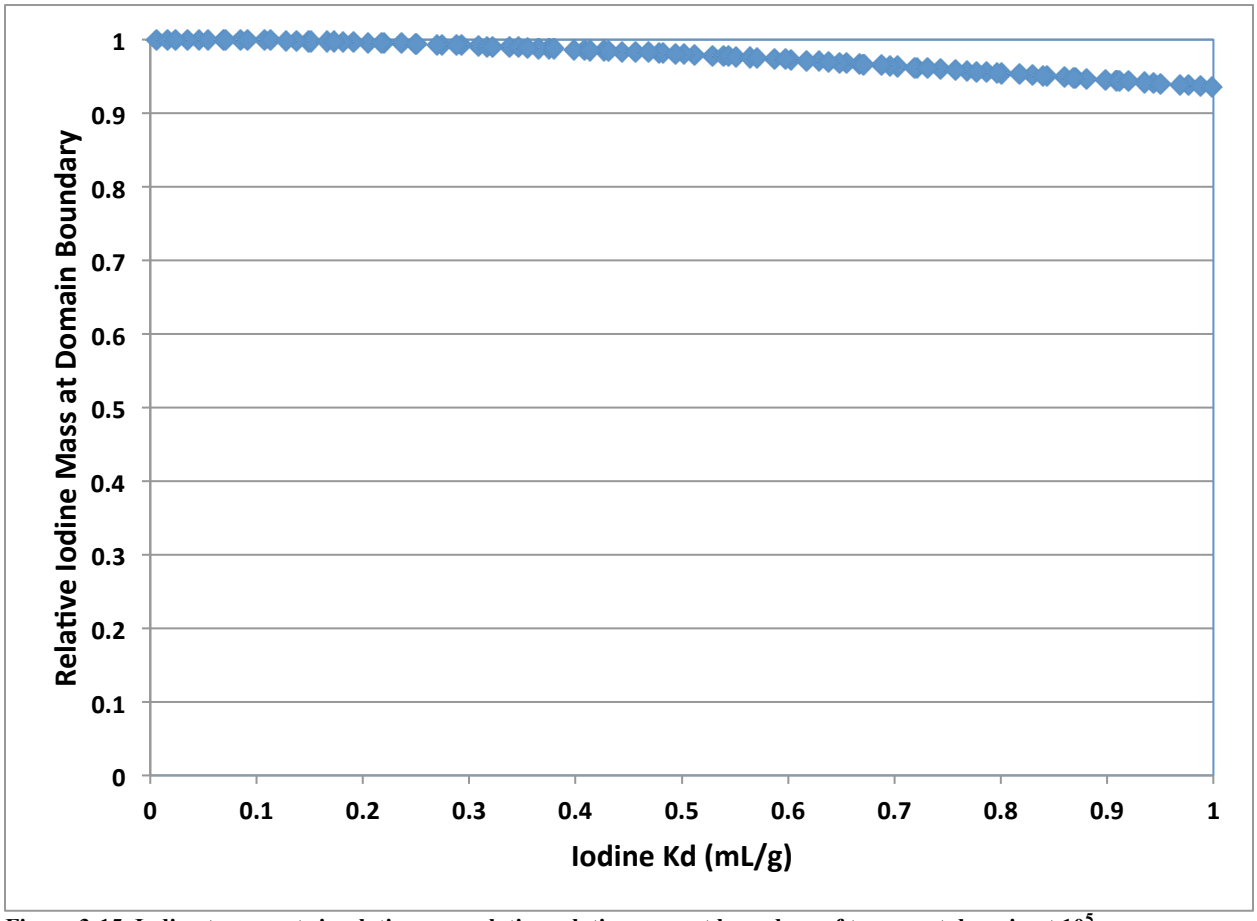


**Figure 3-15. Iodine transport simulation: cumulative relative mass at boundary of transport domain at $10^5$ years versus sorption (Kd) for the probabilistic simulation case**

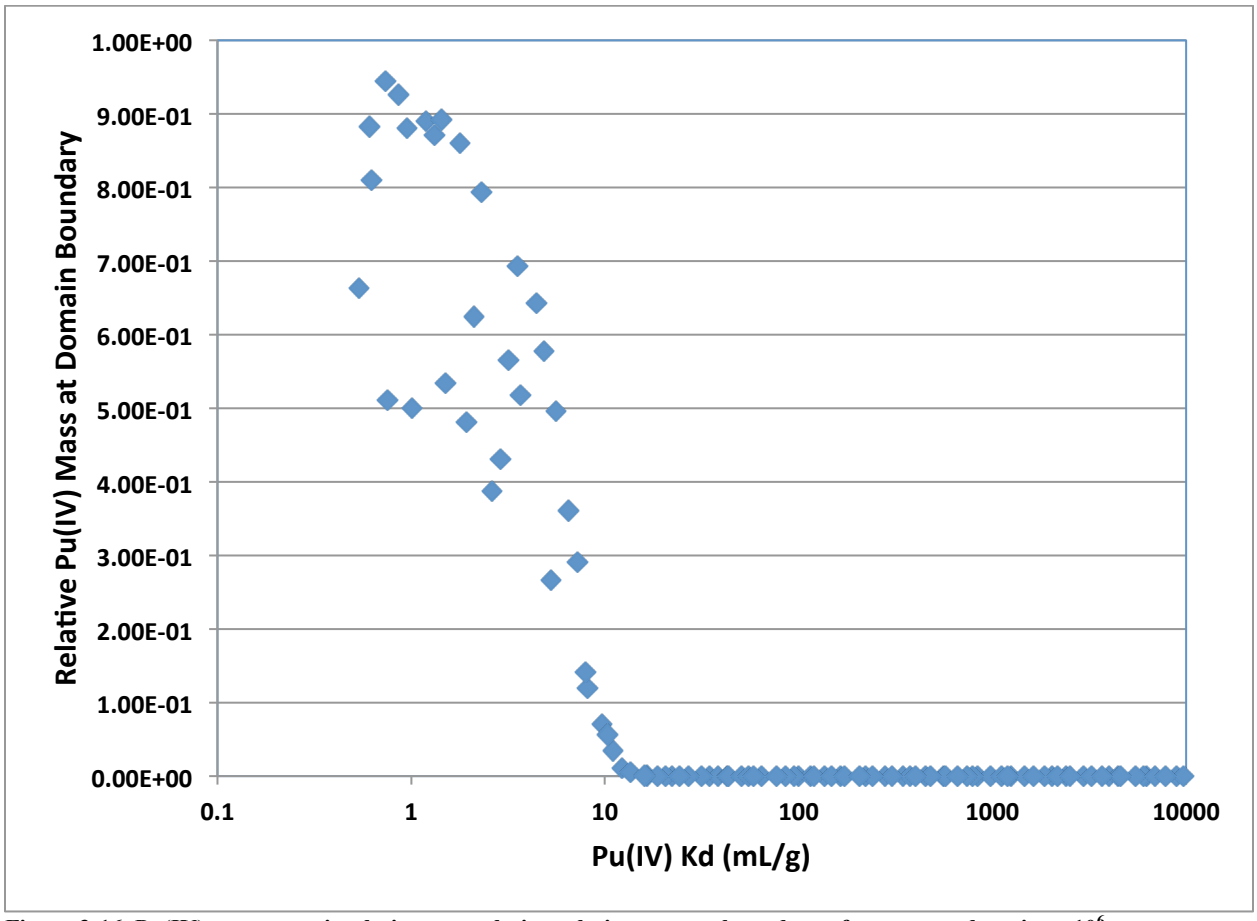


**Figure 3-16. Pu(IV) transport simulation: cumulative relative mass at boundary of transport domain at $10^6$ years versus sorption (Kd) for the probabilistic simulation case**

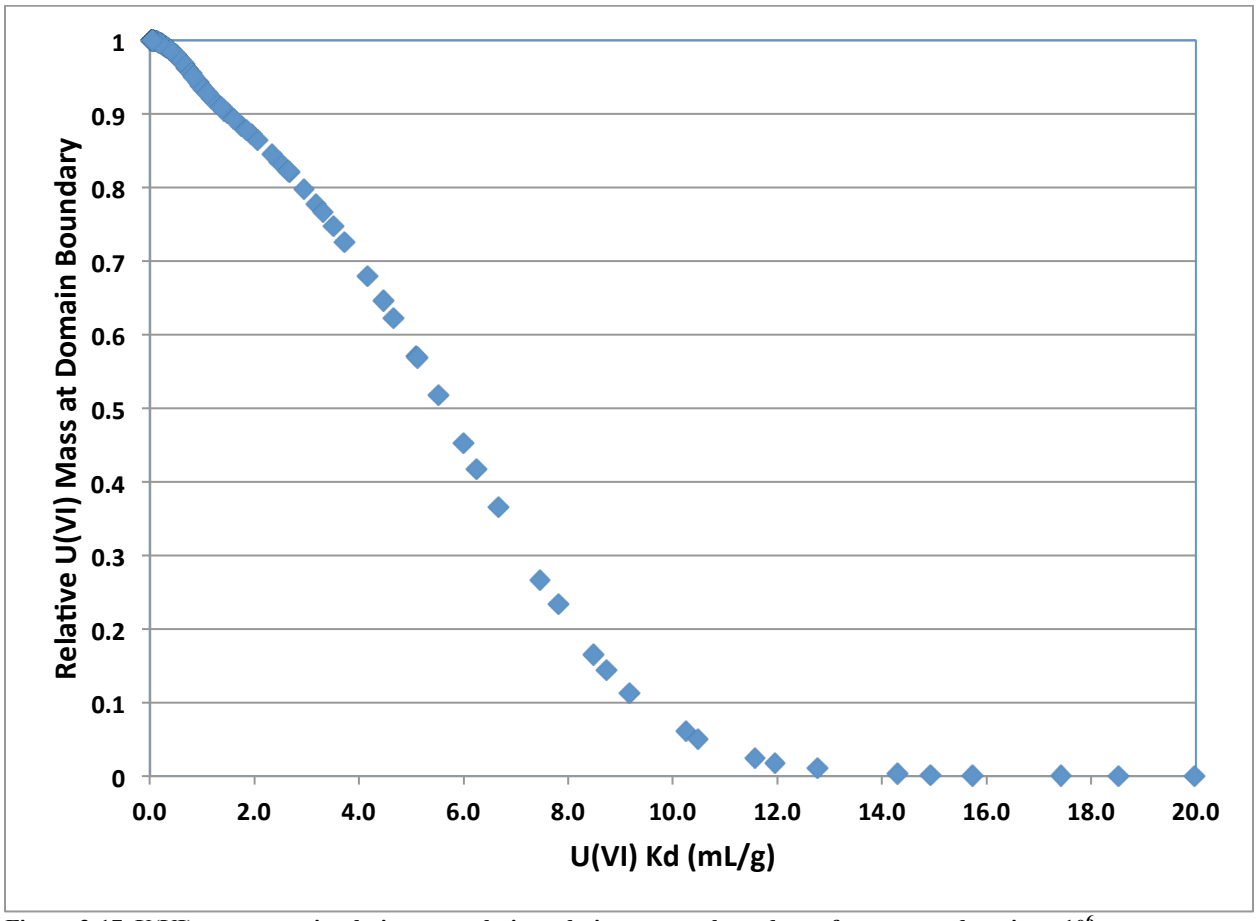


**Figure 3-17. U(VI) transport simulation: cumulative relative mass at boundary of transport domain at $10^6$ years versus sorption (Kd) for the probabilistic simulation case**

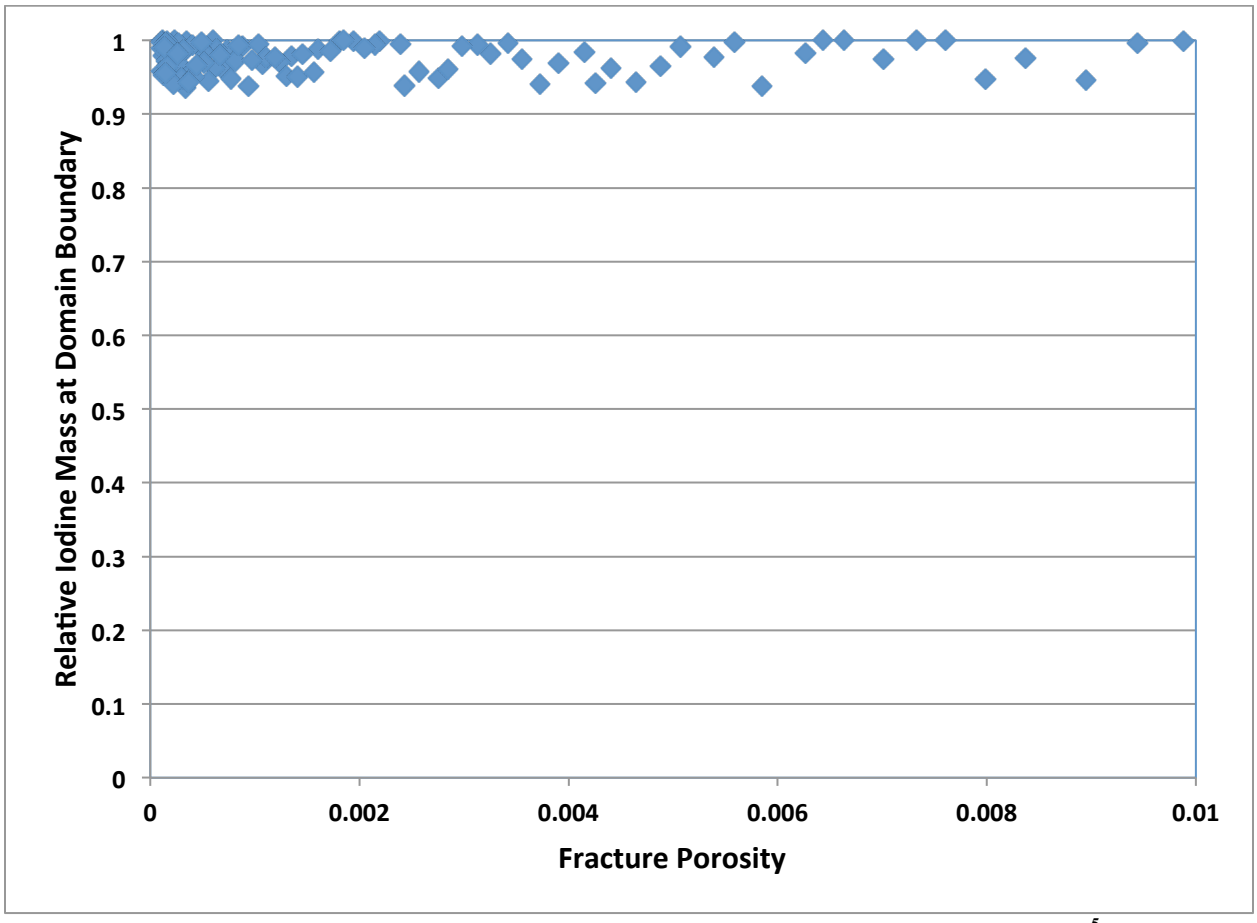


**Figure 3-18. Iodine transport simulation: cumulative relative mass at boundary of transport domain at $10^5$ years versus fracture porosity for the probabilistic simulation case**

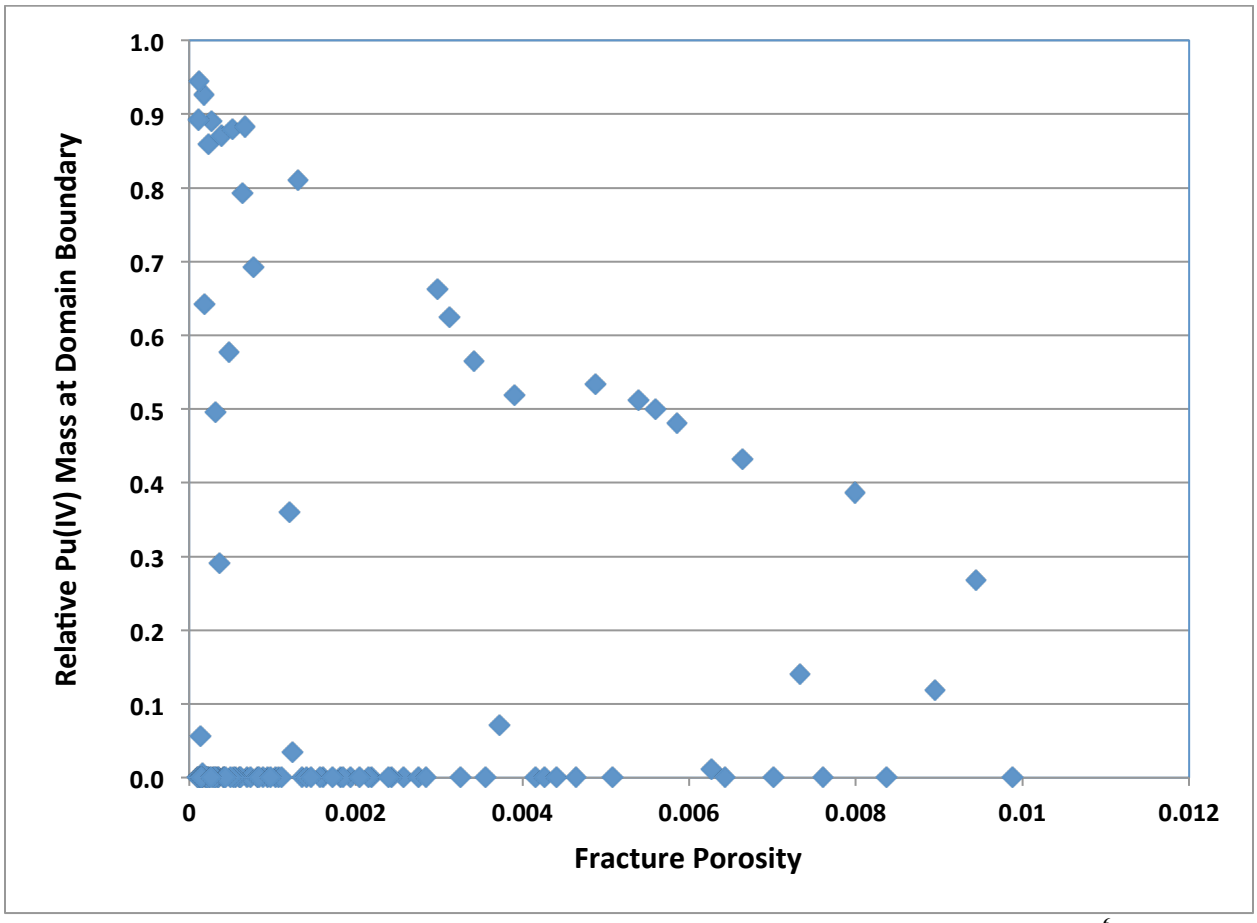


**Figure 3-19. Pu(IV) transport simulation: cumulative relative mass at boundary of transport domain at $10^6$ years versus fracture porosity for the probabilistic simulation case**

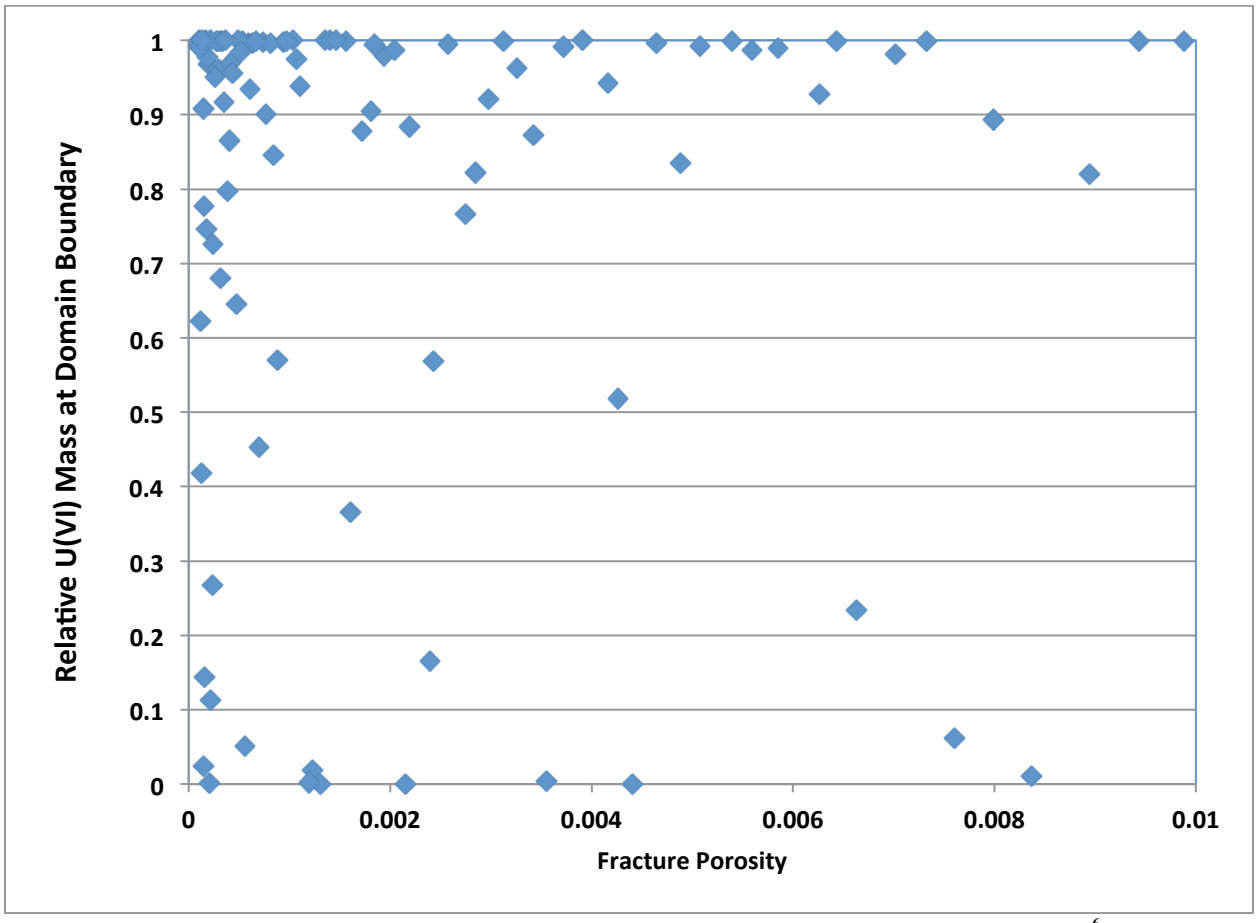


**Figure 3-20. U(VI) transport simulation: cumulative relative mass at boundary of transport domain at $10^6$ years versus fracture porosity for the probabilistic simulation case.**

**Table 3-2. DAKOTA output of statistical data for radionuclide transport**

**Moment-based statistics for each response function:**

| | Mean | Std Dev | Skewness | Kurtosis |
|---|---|---|---|---|
| **response_fn_1** | -4.0225165651e+09 | 8.7810390550e+07 | -2.0057398414e+00 | 3.4229430719e+00 |
| **response_fn_2** | -5.8583954312e+06 | 4.4117471382e+06 | -4.2912685820e-01 | -1.319296085e+00 |
| **response_fn_3** | -2.5824465156e+08 | 9.0697053047e+07 | -2.0048444494e+00 | 3.4182640541e+00 |

**95% confidence intervals for each response function:**

| | LowerCI_Mean | UpperCI_Mean | LowerCI_StdDev | UpperCI_StdDev |
|---|---|---|---|---|
| **response_fn_1** | -4.0399400516e+09 | -4.0050930786e+09 | 7.7098124000e+07 | 1.020071578e+08 |
| **response_fn_2** | -6.7337817770e+06 | -4.9830090854e+06 | 3.8735441876e+06 | 5.125017483e+06 |
| **response_fn_3** | -2.7624091457e+08 | -2.4024838855e+08 | 7.9632633433e+07 | 1.053605222e+08 |

**Simple Correlation Matrix among all inputs and outputs:**

| | kdi | p1 | kdp | kdu | response_fn_1 | response_fn_2 | response_fn_3 |
|---|---|---|---|---|---|---|---|
| **kdi** | | 1.00000e+00 | | | | | |
| **p1** | | -9.36507e-02 | 1.00000e+00 | | | | |
| **kdp** | | -1.71602e-01 | 7.92709e-04 | 1.00000e+00 | | | |
| **kdu** | | -3.24330e-02 | 1.28524e-02 | 1.82083e-02 | 1.00000e+00 | | |
| **response_fn_1** | 9.3593e-02 | -1.0000e+00 | -6.68287e-04 | -1.29001e-02 | 1.00000e+00 | | |
| **response_fn_2** | -4.588e-02 | 1.40320e-01 | -1.34797e-02 | -8.40429e-02 | -1.39908e-01 | 1.00e+00 | |
| **response_fn_3** | 9.3575e-02 | -9.99999e-01 | -6.26540e-04 | -1.29090e-02 | 1.00000e+00 | -1.39791e-01 | 1.0e+00 |

**Partial Correlation Matrix between input and output:**

| | response_fn_1 | response_fn_2 | response_fn_3 |
|---|---|---|---|
| **kdi** | -4.92344e-02 | -3.87679e-02 | -4.82045e-02 |
| **p1** | -1.00000e+00 | 1.37848e-01 | -9.99999e-01 |
| **kdp** | 1.50925e-01 | -1.86882e-02 | 1.51438e-01 |
| **kdu** | -6.65676e-02 | -8.76128e-02 | -5.97702e-02 |

**Simple Rank Correlation Matrix among all inputs and outputs:**

| | kdi | p1 | kdp | kdu | response_fn_1 | response_fn_2 | response_fn_3 |
|---|---|---|---|---|---|---|---|
| **kdi** | 1.0000e+00 | | | | | | |
| **p1** | -2.137e-02 | 1.00000e+00 | | | | | |
| **kdp** | -4.476e-03 | -6.8646e-03 | 1.00000e+00 | | | | |
| **kdu** | -9.2409e-03 | 5.23252e-03 | 4.08041e-02 | 1.00000e+00 | | | |
| **response_fn_1** | 2.1374e-02 | -1.0000e+00 | 6.86469e-03 | -5.23252e-03 | 1.00000e+00 | | |
| **response_fn_2** | -6.0690e-02 | -4.53297e-01 | -1.83942e-01 | -5.11611e-02 | 4.53297e-01 | 1.00000e+00 | |
| **response_fn_3** | 2.1374e-02 | -1.0000e+00 | 6.86469e-03 | -5.23252e-03 | 1.00000e+00 | 4.53297e-01 | 1.00000e+00 |

**Partial Rank Correlation Matrix between input and output:**

| | response_fn_1 | response_fn_2 | response_fn_3 |
|---|---|---|---|
| **kdi** | -1.17147e-02 | -8.22851e-02 | -1.56187e-02 |
| **p1** | -1.00000e+00 | -4.65059e-01 | -1.00000e+00 |
| **kdp** | -3.22341e-03 | -2.09112e-01 | 5.08319e-02 |
| **kdu** | 2.47344e-03 | -4.81514e-02 | 1.57575e-02 |

## 3.3 Summary

The work documented in this section is a continuation of the work of Wang et al. (2012, Section 3) on integration tool development. Wang et al. (2012, Section 3) reported on the development of a prototype PA tool by wrapping a multi-phase, multi-component reservoir simulator (FEHM) with an uncertainty quantification and optimization code (DAKOTA). In this report further development of the PA tool is presented. In this study the flow and transport simulator FEHM was replaced by a multi-phase, multi-

component, and multiscale reactive flow and transport reservoir simulator (PFLOTRAN). PFLOTRAN runs on massively parallel computing system, allowing large scale and faster simulations using the coupled DAKOTA-PFLOTRAN codes. For demonstration of the newly coupled codes, a probabilistic PA analysis was performed for radionuclide transport in the far field of a salt repository. As in Wang et al. (2012, Section 3) the tool demonstration was applied to a far field system with ample field data, and exercised the modeling tools of single-porosity transport (PFLOTRAN), parallel execution (DAKOTA), LHS sampling (DAKOTA), and statistical analysis (DAKOTA).

Further work would include applying dual-porosity radionuclide transport, decay and ingrowth of radionuclides, evaluation of numerical dispersion, and optimization of the key parameters in far-field radionuclide transport system as outlined in Figure 3-1. When directly solving advection-diffusion equations, as was done in this study, use of larger cell sizes may introduce numerical dispersion. Thus, a grid sensitivity study to determine effect of numerical dispersion is warranted. As PFLOTRAN is a massively parallel code, and it was run on Sandia's high performance computing system, reducing mesh size would not be a problem. Numerical dispersion may also be minimized with the applications of other discretization schemes in PFLOTRAN. Further work would also include exercising additional tools within DAKOTA to evaluate the optimal solution for key parameters.

**Acknowledgement**

The authors sincerely thank Glenn Hammond and Satish Kara for providing PFLOTRAN support.

## 3.4 References

Adams, B. M., Bohnhoff, W. J., Dalbey, K. R., Eddy, J. P., Eldred, M. S., Gay, D. M., Haskell, K., Hough, P. D., and Swiler, L. P., 2010. DAKOTA, A Multilevel Parallel Object-Oriented Framework for Design Optimization, Parameter Estimation, Uncertainty Quantification, and Sensitivity Analysis, Version 5.0+ User's Manual, SAND2010-2183, Sandia National Laboratories, Albuquerque, NM.

Balay S, Eijkhout V, Gropp WD, McInnes LC and Smith BF (1997) Modern Software Tools in Scientific Computing, Eds. Arge E, Bruaset AM and Langtangen HP (Birkhaüser Press), pp. 163–202.

Eldred, M., Giunta, A., van Bloemen Waanders, B., Wojtkiewicz, Jr., S., Hart, W., and Alleva, M., 2002, DAKOTA, A Multilevel Parallel Object-Oriented Framework for Design Optimization, Parameter Estimation, Uncertainty Quantification, and Sensitivity Analysis. Version 3.0 Users Manual, SAND2001-3796, Sandia National Laboratories, Albuquerque, NM.

GE Nuclear Energy, 1989. Chart of the Nuclides: Nuclides and Isotopes: Fourteenth Edition.

Hammond, G.E., P.C. Lichtner, C. Lu, and R.T. Mills (2011) PFLOTRAN: Reactive Flow & Transport Code for Use on Laptops to Leadership-Class Supercomputers, Editors: Zhang, F., G. T. Yeh, and J. C. Parker, Ground Water Reactive Transport Models, Bentham Science Publishers. ISBN 978-1-60805-029-1.

Lichtner, P. C. and Hammond, G., 2012. Quick reference Guide: PFLOTRAN 2.0 (LA-CC-09-047) Multiphase-Multicomponent-Multiscale Massively Parallel Reactive Transport Code, report LA-UR-06-7048, Los Alamos National Laboratory, Los Alamos, New Mexico.

Miller, A. W. and Wang, Y., 2012. Radionuclide Interaction with Clays in Dilute and Heavily Compacted Systems: A Critical Review. *Environ. Sci. Technol*. 2012, p. 46.

Wang, Y., Dewers, T., Hadgu, T., Jove-Colon, C. F., Sun, A. C., and McNeish, J. 2010. Enhanced Performance Assessment System (EPAS) for Carbon Sequestration. SAND2010-6173, Sandia National Laboratories, Albuquerque, NM.

Wang, Y., Hadgu, T., Painter, S., Harp, D. R., Chu, S., Wolery, T. and Houseworth, J., 2012. Integrated Tool Development for Used Fuel Disposition Natural System Evaluation – Phase I Report by September 28, 2012, FCRD-UFD-2012-000229, SAND2012-7073P. Milestone: M2FT-12SN0807081, Work Package: FT-12SN080708.

Zyvoloski, G.A. 2007. *FEHM: A control volume finite element code for simulating subsurface multi-phase multi-fluid heat and mass transfer*. Los Alamos Unclassified Report LA-UR-07-3359. Los Alamos, NM: Los Alamos National Laboratory.

Zyvoloski, G.A., B.A. Robinson, Z.V. Dash, and L.L. Trease 1997. *Summary of the models and methods for the FEHM application A Finite-Element Heat- and Mass-Transfer Code*. LA-13307-MS. Los Alamos, NM: Los Alamos National Laboratory.

# 4. Summary and Future Work

This report documents work to develop and demonstrate integrated modeling frameworks that can be used to systematically analyze the performance of a natural barrier system and identify key factors that control the performance of the subsystem. This framework is designed as an integrated tool for prioritization and programmatic decisions of UFDC natural system R&D activities.

Two example simulations were completed in FY2013, one addressing flow and transport in the geosphere of a hypothetical granite repository and one focused on the geosphere of a hypothetical salt repository. The two modeling frameworks share common elements. They both use the parallel subsurface modeling code PFLOTRAN for flow and couple PFLOTRAN to uncertainty analyses tools. The approaches differ in the treatment of transport. A particle-based strategy was used for radionuclide transport in the generic granite example, whereas a parallel solution to the advection-dispersion equation was used in the generic salt repository example.

Taken together, the two example demonstrate the following capabilities:

1. Use of a parallel and highly scalable flow and transport code in integrated assessments to improve realism.
2. Sequential coupling of several process models in a model chain that is both flexible and customized to the integrated assessment problem.
3. Use of uncertainty analysis software to drive the higher fidelity process models.
4. Incorporation of indirect data to constrain uncertainty assessments.
5. Use of unstructured grids to realistically represent complex subsurface structure in the integrated assessments.
6. Use of very efficient and robust particle-based methods specifically designed for probabilistic transport assessments.

The modeling strategies developed and tested here may be useful as one component in future total system modeling frameworks for disposal systems. Extending the framework to represent an engineered barrier system and surface ecological system (biosphere) are potential directions for future work. Other promising directions include more realistic representations of transport processes, including the effects of flow and geochemical transients, and explicit representation of discrete fractures in the transport analyses.